Title
Role of Gas-Phase Halogen Bonding in Ambient Chemical Ionization Mass Spectrometry Utilizing Iodine

Journal
ACS Earth and Space Chemistry, 3(7)

ISSN
2472-3452

Authors
Ganske, Jane A
Wingen, Lisa M
Perraud, Véronique
et al.

Publication Date
2019-07-18

DOI
10.1021/acsearthspacechem.9b00030

Peer reviewed

ACS EARTH AND SPACE CHEMISTRY

Article

Cite This: ACS Earth Space Chem. 2019, 3, 1315−1328

http://pubs.acs.org/journal/aesccq

Role of Gas-Phase Halogen Bonding in Ambient Chemical Ionization Mass Spectrometry Utilizing Iodine

Jane A. Ganske,*,† Lisa M. Wingen,‡ Véronique Perraud,‡ and Barbara J. Finlayson-Pitts‡

†Department of Chemistry, Pepperdine University, 24255 Pacific Coast Highway, Malibu, California 90263, United States

‡Department of Chemistry, University of California, Irvine, Irvine, California 92697-2025, United States

Supporting Information

ABSTRACT: Ambient ionization processes are becoming more widely used for the measurement of atmospherically relevant particles and gases. We report here ambient ionization mass spectra utilizing a commercial tincture of iodine and a piezoelectric discharge gun (PDG) to generate the ionizing reagents. Analytes include Cl_2, Br_2, HNO_3, the C_1−C_9 series of saturated monocarboxylic acids, benzoic acid, 2,2-dimethylpropanoic acid, 9-decenoic acid, and trichloroacetic acid. While Cl_2 and Br_2 form the $[M + I]^-$ iodide adducts, HNO_3 and the organic acids show unexpected peaks corresponding to $[2M - 2H + I]^-$. For HNO_3, the new ion formed is interpreted as the $[NO_3^-\cdots IONO_2]$ complex, where $IONO_2$ is likely formed upon reaction of HOI with gaseous NO_3^-. Similarly, for the organic acids, the $[2M - 2H + I]^-$ peaks are interpreted as $[RC(O)O^-\cdots IOC(O)R]$ complexes formed by association of $RC(O)O^-$ with acyl hypoiodites [RC(O)OI]. It is proposed that the association of (1) Cl_2 and Br_2 with I^-, (2) $IONO_2$ with NO_3^- ions, and (3) RC(O)OI with carboxylate ions occurs via non-covalent halogen bonding. The results suggest the possibility that halogen bonding may play a role in chemical transformations in the atmosphere, particularly in particles where concentrations of iodinated species may be significant.

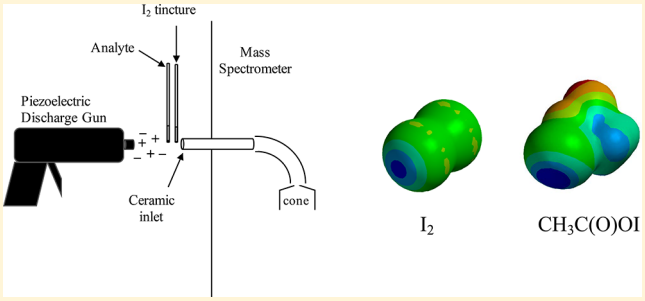

KEYWORDS: *halogen bonding, ambient ionization, plasma discharge gun, iodine, chemical ionization mass spectrometry, acyl hypoiodite*

INTRODUCTION

An extensive set of ion−molecule reactions forms the basis for ionization prior to mass spectrometry detection of atmospherically relevant species. One approach relies on a single ion attaching to an analyte gas [chemical ionization mass spectrometry (CIMS)],[1−7] while another uses a series of more complex ion−molecule reactions [e.g., atmospheric pressure chemical ionization (APCI), and ambient ionization mass spectrometry]. In the first case, chemical ionization reagents, such as ethanol and/or acetone, have been used for the detection of atmospheric amines and amides,[8−10] nitrate ions for detection of sulfuric acid[11,12] and highly oxygenated molecules (HOMs),[13,14] CF_3O^- ions for the detection of hydroperoxides[15] and organic nitrates,[16] SF_6^- ions for the detection of nitric acid and SO_2[17,18] as well as organic acids,[19] acetate ions for the detection of inorganic and organic acids,[20−22] and Cl_3^- and SiF_5^- for the detection of nitric acid.[23,24] Most relevant to the current work is iodide chemical ionization mass spectrometry (I^- CIMS), where the analyte M clusters with iodide ions to form $[M + I]^-$ adducts.[18,25−32] This technique has been used to measure halogen compounds in air[30,32−40] as well as many other inorganic and organic compounds.[1,18,29,31,35,41−47]

A number of emerging methods that fall into the ambient ionization category[3,48−52] are seeing increased use in the field of atmospheric chemistry. Among these are direct analysis in real time mass spectrometry (DART−MS), extractive electrospray ionization mass spectrometry (EESI−MS), and easy ambient sonic spray ionization mass spectrometry (EASI−MS). The advantage of these methods is being able to analyze a variety of samples without the need for collection or sample workup, such as particles on the fly[53−59] and gases.[60−66] Because the ionization is generally carried out at atmospheric pressure in room air, other trace species in addition to the analyte are ionized concomitantly. If these species occur in a high enough concentration, they may alter the ionization of the analyte,[60] but with care, these complications can be minimized and taken into account.

Some of these ambient methods rely on plasmas to generate the ionization agents.[2,51,52,67−70] One such plasma source utilizes a piezoelectric discharge, which has been used to vaporize and ionize analytes in a stream of liquid solvent[71] and to identify gaseous contaminants in room air.[60] Piezoelectric discharge guns (PDGs) are inexpensive and widely available because they are used to remove static charges from surfaces.

Received: February 8, 2019
Revised: May 15, 2019
Accepted: May 16, 2019
Published: June 7, 2019

DOI: 10.1021/acsearthspacechem.9b00030
ACS Earth Space Chem. 2019, 3, 1315−1328

The PDG generates a pulse of both positive ions (trigger compression) and negative ions (trigger release) in a single manual "squeeze and release" cycle via mechanical distortion of a piezoelectric element. Previous studies have shown that ionization using piezoelectric devices results in soft ionization similar to DART or APCI, typically involving the addition of a proton from protonated water clusters or removal of a proton by O_2^-.[60,71,72]

We report here studies of PDG ionization of an I_2 tincture to detect Cl_2, Br_2, HNO_3, and a series of organic acids. These analytes are atmospherically significant in different ways. The halogens are important in the atmospheric oxidant cycle[73−78] because they photolyze to form highly reactive chlorine or bromine atoms, leading to ozone formation or destruction, respectively. Nitric acid is important as a temporary reservoir to tie up highly reactive oxides of nitrogen in air, which would otherwise lead to the formation of ozone and other manifestations of photochemical air pollution.[79] Organic acids are commonly found in particles in air, arising from direct emissions and as products of oxidation of volatile organic compounds.[80−82]

We show that, while iodide adducts (i.e., $[M + I]^-$ ions) are formed with the halogens as observed previously in CIMS studies,[30,33−40] organic acids are detected via a different ionization chemistry. In both cases, the adducts observed demonstrate a role for halogen bonding in the gas phase. Halogen bonding is a non-covalent interaction between a positively polarized region of a halogen atom in a molecule and a nucleophilic region of a molecule (or anion).[83,84] For example, molecular iodine shows an anisotropic electron density, with regions of negative potential on the equatorial sides on the halogen atoms and positive electrostatic potentials at the ends of the bond axis to form what is called a sigma (σ) hole[83−91] (Figure 1) that halogen bonds to nucleophiles.

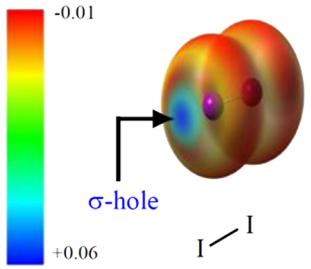

Figure 1. Electrostatic potential diagram showing a region of positive electrostatic potential, the σ hole, in molecular iodine. This figure was adapted with permission from ref 91. Copyright 2018 John Wiley & Sons, Inc.

Conceptually similar to a hydrogen bond, halogen bonding has been widely observed in many different contexts, including molecular self-assembly, drug design, organic synthesis, and biomolecular systems.[83,87,92,93] Here, we suggest that the halogen bonding phenomenon plays an important role in the analyte clusters formed when PDG ionization of iodine tincture serves as the reagent source. Possible implications for a role of halogen bonding in atmospheric systems are discussed.

EXPERIMENTAL SECTION

Chemical Ionization by PDG Plasma. A hand-held PDG (Milty Zerostat 3 antistatic gun, Armour Home, Bishops Stortford, U.K.) was used as an open-air ionization source at the inlet of a mass spectrometer (Figure 2). The negative ion trigger release was used to ionize samples at the tip of two open capillaries held in air about 1 mm from the inlet of the mass spectrometer. The capillaries were microhematocrit tubes coated with ammonium heparin (VWR), for which the coating was removed by sonication in nanopure water (18 MΩ cm, Thermo Scientific, Barnstead), and the capillaries dried before use. Uncoated melting point capillaries were used with similar results. The capillaries were situated perpendicularly to the inlet of a triple quadrupole mass spectrometer (Xevo TQ-S, Waters, Milford, MA, U.S.A.) operated in negative ion mode. One capillary contained the I_2 tincture, while the second contained the analyte. A selected number of experiments were also performed using methyl iodide (CH_3I), instead of the I_2 tincture as the reagent. For all experiments, a DART−MS ionization source (IonSense) equipped with the Vapur interface and a 6 cm long ceramic tube (inner diameter of 4.75 mm) was used as the MS inlet interface. The PDG replaced the helium DART probe as the ionization source, and the two capillary tubes were located in between the PDG source and the inlet of the mass spectrometer. Mass spectra were collected in negative ion mode from either a single discharge of the PDG or averaged over 2−8 slow trigger releases and analyzed using MassLynx software. For comparison, some spectra were collected with the DART−MS probe located 4 cm away from the MS inlet. DART was operated with helium reagent gas at a flow of 3.1 L min^{-1}, a He gas temperature of 150 °C, and a grid electrode voltage of −350 V in the negative ion mode.

For both methods, specific in-source parameters were as follows: cone voltage, 30 V; source offset, 50 V; no cone gas; and ion block temperature, 110 °C. These are the values set in the MassLynx software and are not absolute values with respect to ground. The inside of the ceramic tube as well as the Vapur interface were at atmospheric pressure, while the pressure behind the 0.8 mm sample cone controlled by a rough pump (i.e., ion block and T-wave region as illustrated in Figure 2) was ∼2 mbar. The pressure in the ion guide region was maintained at (7−8) × 10^{-3} mbar, while the analyzer was operated at 1 × 10^{-5} mbar. Full mass spectra were acquired over 0.1 or 1 s using the second quadrupole, while the first quadrupole and collision cell acted as additional ion guides (no scanning or fragmenting). Similar spectra resulted when spectra were acquired over 0.1, 0.25, or 1 s, with improved time resolution and sensitivity obtained at faster scan rates. Improved time response was due to the better synchronization between ion bursts accompanying trigger release and MS collection with faster scan rates (see Figure S1 of the Supporting Information). The collision cell energy was typically set to 2 eV for full mass spectra, with some spectra collected using 15 eV as discussed in the Supporting Information. In separate experiments, MS/MS scans were acquired with various collision energies (2−30 eV) applied to the collision cell to investigate the fragmentation of a given species. Argon gas flow in the collision cell was maintained at 0.15 mL min^{-1} in both full MS scan and MS/MS scans.

Because static electricity removal devices are known to generate ozone as a result of the high voltages produced (3−8 kV), ozone concentrations after repeated gun squeeze/release cycles were measured using a photometric ozone analyzer (model 400E, Teledyne API) at approximately the same

DOI: 10.1021/acsearthspacechem.9b00030
ACS Earth Space Chem. 2019, 3, 1315−1328

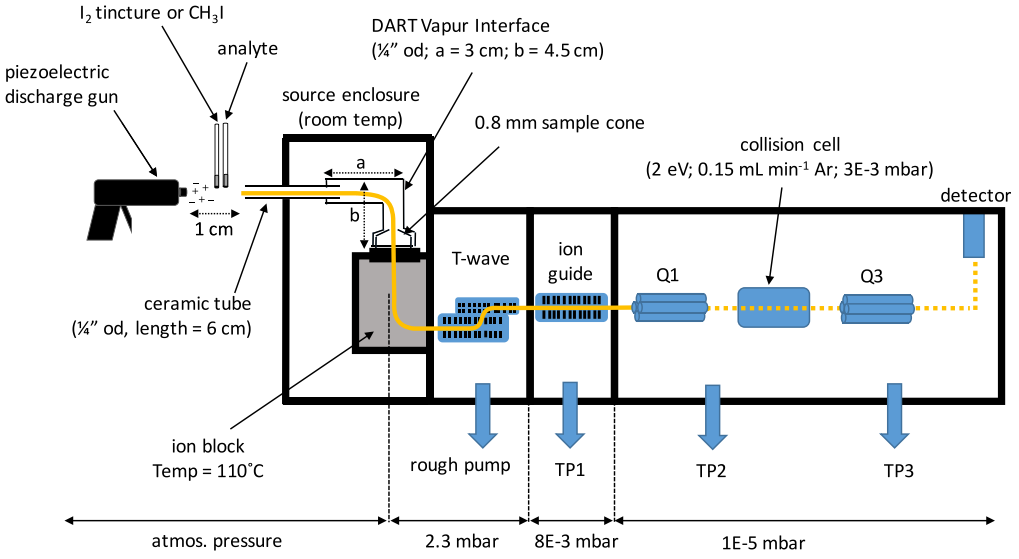

Figure 2. Schematic diagram of the mass spectrometer and source region including the placement of the PDG and sample capillaries.

distance as that between the PDG and the mass spectrometer inlet in the experiments.

Chemicals and Reagents. Iodine tincture solutions containing approximately 2% (w/w) I_2 and 2% (w/w) NaI in aqueous ethanol were obtained commercially (Walgreens) or prepared in the laboratory. In the latter case, the solution was allowed to equilibrate for several hours to establish iodide ion equilibria (*vide infra*). Iodine (>99.8%, ACS grade, Fisher Chemical), sodium iodide (≥99.5%, EMD), and ethanol (200 proof, Goldshield Chemical Company) were used as received. Methyl iodide was purchased from Sigma-Aldrich (99%).

All acids were used as received: nitric acid (69% certified ACS plus, Fisher), formic acid (88%, Fisher), acetic acid (glacial 99.7%+, EMD), propanoic acid (99%+, Mallinckrodt), butanoic acid (99.5%, anhydrous, Sigma), pentanoic acid (99% +, Sigma-Aldrich), hexanoic acid (99.5%+, Sigma-Aldrich), heptanoic acid (99%+, Sigma-Aldrich), octanoic acid (99%, Sigma-Aldrich), nonanoic acid (96%, Sigma-Aldrich), 2,2-dimethylpropanoic (99%, Sigma-Aldrich), benzoic acid (99.5%, Sigma-Aldrich), 9-decenoic acid (95%+, Narchem), and trichloroacetic acid (99%+, Sigma-Aldrich). Liquid bromine (99.5%, ACS reagent grade) was purchased from Sigma-Aldrich, and a standard gas mixture of Cl_2 [10.58 ppm of Cl_2 (±5%) in N_2, AirGas Specialty Gases] was also used.

RESULTS AND DISCUSSION

Negative Ion Mass Spectra in the Absence of Analytes. Figure 3a shows the negative ion mode mass spectrum generated by PDG ionization in laboratory air with no iodine reagents present. The inset in Figure 3a shows the total ion count as a function of time during PDG trigger release, demonstrating both the variability and signal-to-noise ratios of the method. Ions are formed and detected only during each PDG trigger release with no background ion signal between these bursts, resulting in very high signal-to-noise ratios. The ions observed are those that have been previously identified in DART and APCI as, e.g., CO_3^- (m/z 60), HCO_3^- (m/z 61), and NO_3^- (m/z 62).[94−97] Lactic acid from human skin vapor gives rise to a peak at m/z 89 [$CH_3CH(OH)$-CO_2^-].[98] The ionization mechanism that occurs for PDG ionization in ambient air (with no added ionization reagent) is shown in Figure S2a of the Supporting Information.

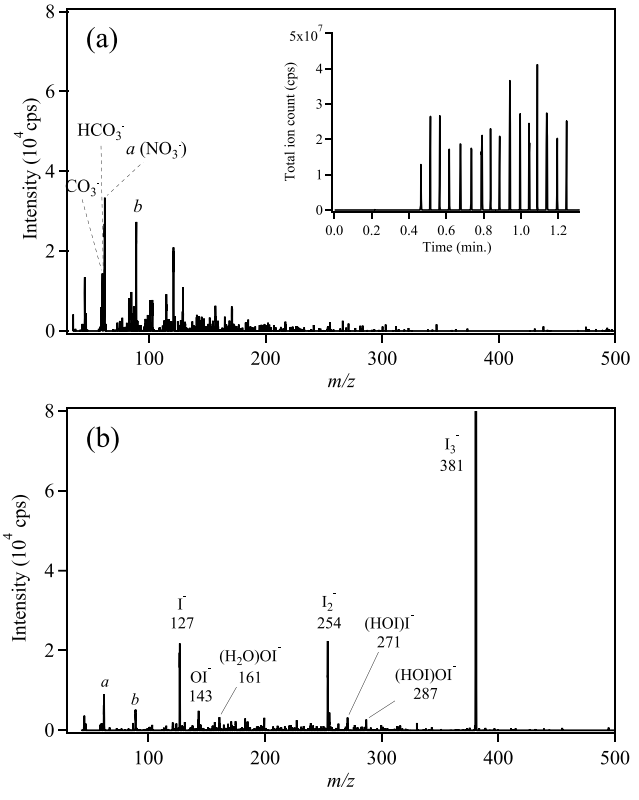

Figure 3. Mass spectra of reagent ions generated by PDG ionization of (a) laboratory air (no reagent) and (b) a commercial iodine tincture. Peaks labeled *a* and *b* at m/z 62 and 89, respectively, are due to NO_3^- and lactic acid $[M - H]^-$ ion, commonly observed in ambient negative ion mode spectra.[94−97] The inset in part a shows the time resolution and reproducibility of PDG total ion counts during several squeezes.

Figure 3b shows a typical negative ion mass spectrum of reagent ions generated by applying the PDG source to a commercial iodine tincture. Dominating the spectrum in Figure 3b are peaks at m/z 127 (I^-), 254 (I_2^-), and 381 (I_3^-),

DOI: 10.1021/acsearthspacechem.9b00030
ACS Earth Space Chem. 2019, 3, 1315−1328

along with smaller but still significant peaks at m/z 143 (OI^-), 161 $(H_2O)OI^-$, 271 $(HOI)I^-$, and 287 $(HOI)OI^-$. A detailed ionization mechanism for the ions observed is illustrated in Figure S2b of the Supporting Information. A small peak IO_3^- (175) was also observed in many cases.

The multiplicity of iodine-containing reagent ions in Figure 3b arises in part from a series of complex equilibria common to aqueous iodine solutions.[99,100] Commercial iodine tinctures used as skin disinfectants contain 2% I_2 in water as well as 2% NaI or KI and ethanol to aid in the dissolution of I_2. An equilibrium between molecular iodine, iodide, and triiodide is established over several hours in the tincture solution (reaction 1).

$$I_2 + I^- \rightleftharpoons I_3^- \quad (1)$$

Molecular iodine hydrolyzes in water to form hypoiodous acid (HOI),[101]

$$I_2 + H_2O \rightleftharpoons HOI + I^- + H^+ \quad (2)$$

which readily disproportionates, forming the iodate ion, IO_3^-, and regenerating iodine.

$$5HOI \rightleftharpoons 2I_2 + IO_3^- + H^+ + 2H_2O \quad (3)$$

Hypoiodous acid is able to partition from aqueous solution to the gas phase [$K_H = (2-5) \times 10^{-3}$ atm M^{-1}],[102,103] although less readily than molecular iodine (K_H = 0.3 atm M^{-1}).[103] Laboratory-prepared solutions containing either molecular iodine or an iodide salt, but not both, did not generate the abundance of iodide reagent ions that the I_2/I^- tincture provided upon ionization. Thus, both I_2 and I^- are important species, suggesting the equilibria in reactions 1−3 are responsible for the generation of reagent ions in these experiments. Supporting these equilibria in the liquid tincture, ultraviolet (UV)-visible measurements of the tincture showed the presence of I_2, I_3^-, and HOI (Figure S3 of the Supporting Information).

The observed iodine species were investigated by collecting full MS scans of the I_2 tincture using PDG and DART−MS ionization at low and high collision cell energies. Panels a and b of Figure S4 of the Supporting Information show that PDG ionization at a collision cell energy of 2 eV yields ion adducts of HOI and OI^- at m/z 161 $(H_2O)OI^-$, 271 $(HOI)I^-$, and 287 $(HOI)OI^-$ (the same as Figure 3b), while a higher collision cell energy of 15 eV leads to their fragmentation. The ions I^-, OI^-, I_2^-, and I_3^- remain dominant at both collision energies. For comparison, DART−MS, which is known to generate O_2^-,[96] was used to collect negative ion mode spectra of the I_2 tincture. Panels c and d of Figure S4 of the Supporting Information show DART−MS spectra using collision cell energies of 2 and 15 eV, respectively. A comparison of DART and PDG ionization at 2 eV shows that the ions generated from the I_2 tincture for both methods of ionization include dominant I^-, I_2^-, and I_3^- ions and small contributions from OI^- and HOI ion adducts. Similarly, the spectra using PDG and DART at a collision cell energy of 15 eV are comparable, in which I^-, I_2^-, and I_3^- remain the major ions, while the HOI and OI^- adducts are fragmented. These data show that the mechanism of ionization provided by piezoelectric ionization in ambient air is analogous to that provided by ionization using DART−MS.[96] The identification of ions at m/z 143 (OI^-), 161 $(H_2O)OI^-$, 271 $(HOI)I^-$, and 287 $(HOI)OI^-$ was confirmed with product ion scans carried out with DART−MS (Figure S5 of the Supporting Information).

While there is considerable variability in the total ion counts of the iodine adducts using PDG from pulse to pulse (inset in Figure 3a), I^- and I_3^- consistently comprise the largest percentage of ion counts in PDG ionization of iodine tincture. The reproducibility of the charge generated during successive squeezes of the PDG is unknown and may contribute to this variability, as could oxidation chemistry in the ionization region involving oxygen and/or ozone. Although a maximum of 607 ppb of O_3 was generated by 30 successive trigger squeeze/release cycles, ozone formation was minimized in experiments reported here using either a single trigger release or an average over 2−8 trigger releases. However, secondary chemistry between ozone and iodide ions may still occur, causing the additional formation of oxyanions and perturbing the equilibria shown in reactions 1−3. Ozone is known to react with aqueous iodide at the air−water interface to generate iodine oxyanions.[104−106] The exposure of aqueous NaI solutions to a flow of ozone at levels above 50 ppb was shown previously to generate oxidized forms of iodine detected by electrospray ionization mass spectrometry (ESI−MS), including OI^-, IO_2^-, and IO_3^-.[105]

To investigate the effect of O_3 on the distribution of ions, a slow flow of several parts per million (ppm) of O_3, generated from 185 nm photolysis of O_2, was introduced during ionization. The peak at m/z 175 (IO_3^-) increased significantly, consistent with known O_3−iodide chemistry. Other oxyanions were not observed. The peak intensities of OI^-, I^-, and I_3^- did not change significantly when several ppm O_3 were present.

For comparison to traditional I^- CIMS studies, in which the ionizing reagent is often formed under slight vacuum and in an inert N_2 atmosphere, PDG ionization of CH_3I was carried out. The major ions observed were I^- with some IO_3^- (Figure S6a of the Supporting Information). It is important for the later discussion to note that there is no OI^- peak at m/z 143 or HOI adducts observed using CH_3I as the precursor. Iodide ion (I^-), its clusters with water, and I_3^- have been reported in I^- CIMS studies employing ionization of CH_3I with discharge processes,[32] X-ray,[107,108] or radioactive sources, such as ^{210}Po.[26,30,33,38,40,109,110] In the case of I^- CIMS using ^{210}Po for example, I^- is generated via dissociative electron attachment to CH_3I. Lee et al.[30] reported the presence of minor ions, such as OI^-, IO_2^-, and IO_3^-, from CH_3I ionization with a ^{210}Po source, and other discharge sources using CH_3I have been reported to generate not only IO_3^- but also OI^-, IO_2^-, and IO_4^-.[32] In electrospray chemical ionization techniques using iodide salt solutions as the reagent ionization source, only I^- and I_3^- are observed.[111,112]

Application to Cl_2 and Br_2. As proof of concept, the PDG ionization technique using the iodine tincture reagent source was applied to gaseous Cl_2 and liquid Br_2. Mass spectra are shown in Figure 4. As expected, both Br_2 and Cl_2 form iodide adducts. This result is not surprising, because Lee et al.[35] reported Cl_2I^- and Br_2I^- clusters from I^- CIMS measurements using CH_3I and suggested that their high polarizabilities (31.36 $bohr^3$ and 46.72 $bohr^3$, respectively) contribute to their strong cluster formation. Thus, peaks as a result of Cl_2I^- are found at m/z 197, 199, and 201, and peaks as a result of Br_2I^- are found at m/z 285, 287, and 289, with the ratios of the peak intensities in both cases as expected from the isotopic abundances of chlorine and bromine.

DOI: 10.1021/acsearthspacechem.9b00030
ACS Earth Space Chem. 2019, 3, 1315−1328

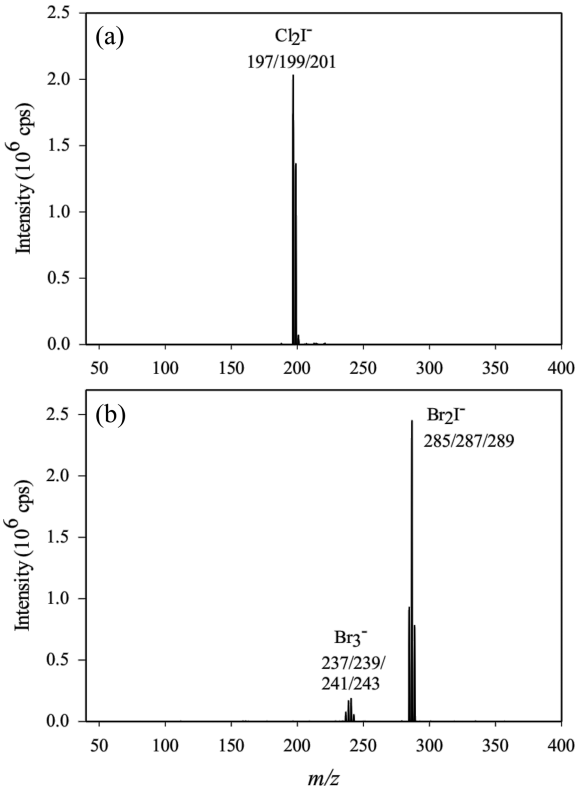

Figure 4. Mass spectrum of (a) gas-phase chlorine and (b) liquid bromine ionized by PDG with the iodine tincture.

The detection of the gaseous trihalide ion adducts I_3^-, Cl_2I^-, Br_2I^-, and Br_3^- (Figures 3b and 4) illustrates the unusual stability of the halogen bond in these adducts. Anionic halogen bond acceptors are generally stronger than neutral species, and the strength of the halogen donor increases in the order Cl < Br < I. Solution-phase triiodide ion is a hallmark example of a halogen bond occurring through a σ hole on molecular iodine interacting with the iodide anion through the $I_2\cdots I^-$ association (180 kJ/mol).[87,89] We assert that this same interaction in the gas phase accounts for the presence of I_3^-, Cl_2I^-, Br_2I^-, and Br_3^- reported here.

Application to Nitric Acid. Figure 5 presents the mass spectrum observed when the headspace of a 15.8 M HNO_3 solution is analyzed using PDG ionization of the I_2 tincture.

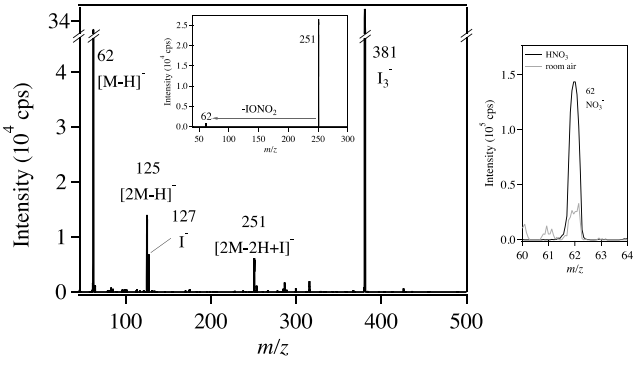

Figure 5. Mass spectrum of PDG-ionized HNO_3 with the iodine tincture. The inset is the product ion scan of m/z 251 acquired at a collision cell energy of 5 eV. For comparison, background NO_3^- ion intensity is shown on the right.

Peaks appear at m/z 62 (NO_3^-, with intensities 5−10 times above background NO_3^- levels) and m/z 125 (corresponding to the $[2M - H]^-$ adduct). These ions, $[M - H]^-$ and $[2M - H]^-$, are expected on the basis of traditional APCI mechanisms. Under the ambient ionization conditions and the high concentrations of HNO_3 used here, the dimer ion is observed. In contrast to the halogens, no $[M + I]^-$ adduct is observed, despite the high binding energy of HNO_3 with I^-.[29,44] However, an unexpected iodide cluster is observed at m/z 251, corresponding to $[2M - 2H + I]^-$.

Product ion scans were performed to examine the fragmentation pattern of the $[2M - 2H + I]^-$ cluster. Using collision energies ranging from 2 to 30 eV, the product ion spectra showed that the cluster at m/z 251 dissociates to NO_3^-, with a neutral loss of iodine nitrate, $IONO_2$ (inset in Figure 5). This is consistent with the formation of $[2M - 2H + I]^-$ via the reaction of NO_3^- with $IONO_2$.

$$NO_3^-(g) + IONO_2(g) \rightarrow [ONO_2\cdots IONO_2]^-(g) \quad (4)$$

Higher collision energies did not induce further fragmentation of $IONO_2$.

The presence of a σ hole on the iodine atoms of I_2 and HOI is known to promote halogen bonding,[113−116] likely with the NO_3^- anion. In this vein, we propose that $IONO_2$ is formed in the gas phase via reactions 5a and 5b.

$$I_2(g) + NO_3^-(g) \rightarrow IONO_2(g) + I^-(g) \quad (5a)$$

$$HOI(g) + NO_3^-(g) \rightarrow IONO_2(g) + OH^-(g) \quad (5b)$$

Supporting I_2 and HOI in the ionization region is the observation in mass spectra (Figure 3b) of I_2^-, OI^-, $(H_2O)OI^-$, $(HOI)I^-$, and $(HOI)OI^-$. The ion OI^- is likely from the deprotonation of HOI. There are other ion−molecule reactions that are possible, which include the reaction of OI^- with nitric acid (reaction 6).

$$OI^-(g) + HNO_3(g) \rightarrow IONO_2(g) + OH^-(g) \quad (6)$$

However, on the basis of thermodynamics (Table S1 of the Supporting Information), OI^- is expected to deprotonate HNO_3 in competition with the potential chemistry in reaction 6). Another possibility is the reaction of HOI ion clusters, such as $HOI(I)^-$, with HNO_3 (reaction 7).

$$HNO_3(g) + HOI(I)^-(g) \rightarrow IONO_2(g) + H_2O(g) + I^-(g) \quad (7)$$

However, the intensities of the HOI clusters are relatively small compared to the NO_3^- peak intensity, suggesting that this is less important. The absence of a $[M + I]^-$ adduct upon HNO_3 analysis with the I_2 tincture suggests that HNO_3 is deprotonated to form NO_3^- upon PDG ionization. Because ambient ionization methods commonly generate O_2^- ions, as in DART and APCI,[95,96] deprotonation of HNO_3 by O_2^- must dominate over adduct formation between HNO_3 and I^- under these ambient conditions. Thus, acids more acidic than HO_2 in the gas phase will be deprotonated by O_2^-, and their anions will be observed in the spectrum (see Table S1 of the Supporting Information).

DART−MS spectra of I_2 tincture in the absence and presence of nitric acid were collected for comparison. Figure S7 of the Supporting Information shows that, when HNO_3 is present, the HOI/OI^- adducts are not observed and peaks at m/z 62, 125, and 251 appear in similar relative ratios observed

DOI: 10.1021/acsearthspacechem.9b00030
ACS Earth Space Chem. 2019, 3, 1315−1328

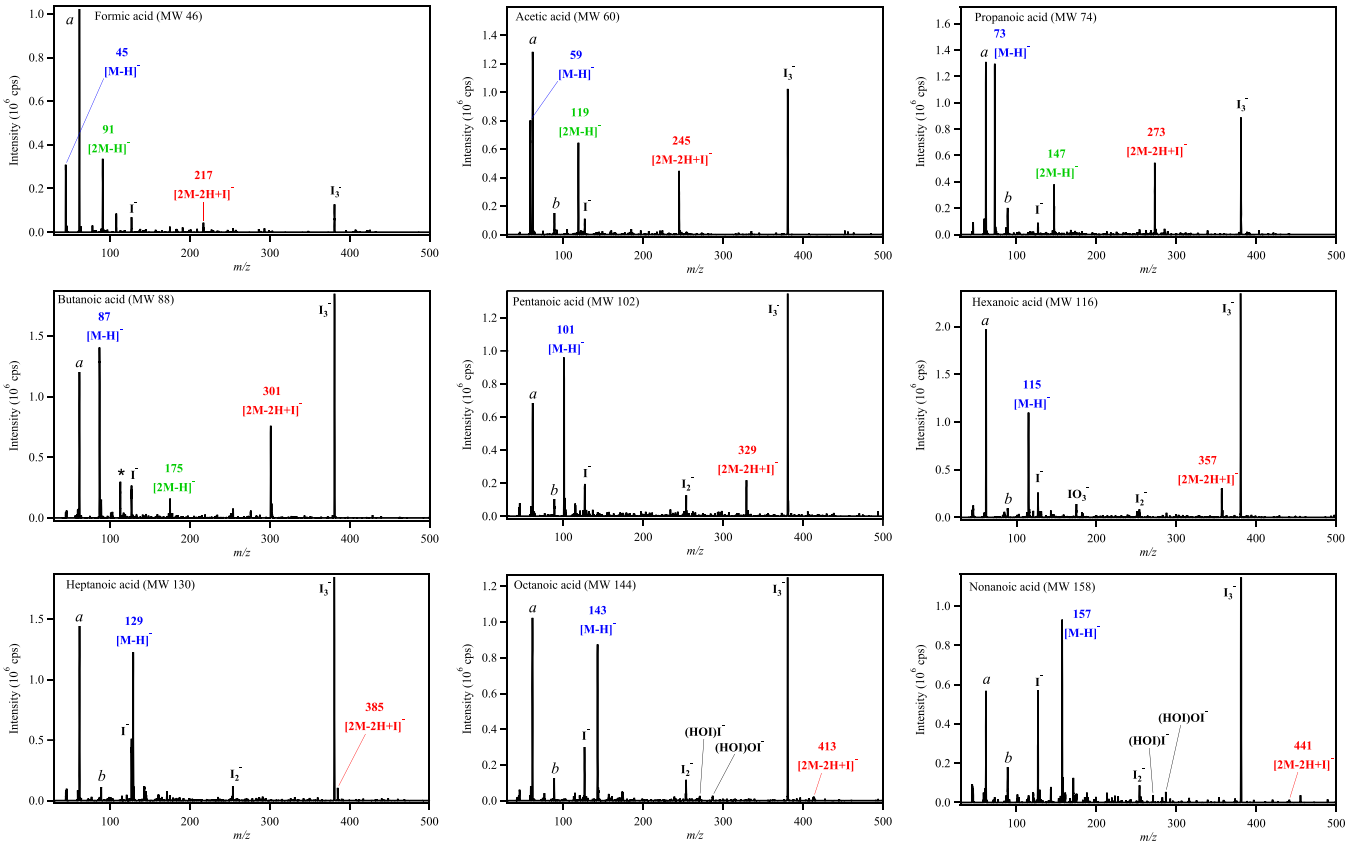

Figure 6. Mass spectra of C_1−C_9 alkanoic acids ionized by PDG with the iodine tincture showing locations of $[M - H]^-$ (blue), $[2M - H]^-$ (green), and $[2M - 2H + I]^-$ (red). The $[2M - H]^-$ adducts for C_5−C_9 are present in each spectrum but too small to be seen with the displayed scale. The I_3^- peak is off scale in some spectra. Peaks labeled *a* and *b* at *m*/*z* 62 and 89, respectively, are due to NO_3^- and lactic acid $[M - H]^-$. A contaminant peak (labeled with an asterisk) was observed at *m*/*z* 113 for butanoic acid.

for PDG ionization (Figure 5). This supports that PDG and DART generate the deprotonating agent, O_2^-, with similar mechanisms and that NO_3^- forms an adduct with both $IONO_2$ to form the $[2M - 2H + I]^-$ cluster and HNO_3 to yield the dimer ion, $[2M - H]^-$.

Application to Monocarboxylic Acids. To assess the ability of PDG-generated ions from the iodine tincture to detect organic acids, a homologous series of monocarboxylic acids (C_1−C_9 alkanoic acids) was investigated. Mass spectra resulting from the simultaneous ionization of each of the C_1−C_9 monocarboxylic acids with the iodine tincture at the mass spectrometer inlet are presented in Figure 6. Spectra are dominated by the $[M - H]^-$ ion (blue labels in Figure 6). This is in contrast to reported I^- CIMS using CH_3I and a ^{210}Po source, where very small carboxylate signals were observed relative to $[M + I]^-$.[30] Peaks corresponding to $[2M - H]^-$ ions (green labels in Figure 6) were also clearly observed for the C_1−C_4 acids. For the $\geq C_5$ acids, the $[2M - H]^-$ ion peaks were very small. However, an unexpected iodide cluster corresponding to $[2M - 2H + I]^-$, appears in the mass spectra of all of the C_1−C_9 acids (red labels in Figure 6) at *m*/*z* 217 (C_1), 245 (C_2), 273 (C_3), 301 (C_4), 329 (C_5), 357 (C_6), 385 (C_7), 413 (C_8), and 441 (C_9).

Product ion scans were again performed to examine the fragmentation patterns of the $[2M - 2H + I]^-$ cluster. Scans were recorded at increasing collision energies ranging from 2 to 30 eV. The product ion spectra of each of the $[2M - 2H + I]^-$ ions for the homologous series showed the corresponding $[M - H]^-$ ion (see two representative MS/MS spectra for acetic and nonanoic acids in Figure S8 of the Supporting Information). From those, a neutral loss of $[M - H + I]$ is observed for all acids and is consistent with the homologous series of the acyl hypoiodites, RC(O)OI.

Acyl hypoiodites are generally regarded as transient species in solution-phase iodination chemistry.[117−119] However, acetyl hypoiodite has recently been detected by gas chromatography−mass spectrometry (GC−MS) in an acetic acid solution containing iodine and *t*-butyl hydroperoxide,[91] and Urbansky et al. postulated the formation of acetyl hypoiodite in solutions of acetic acid, acetate ion, and hypoiodous acid.[120] By analogy to the HNO_3 observations presented above (reactions 5a and 5b), we propose that acyl hypoiodites are formed in the gas phase through the reactions 8a and 8b of I_2 or HOI with $RC(O)O^-$.

$$I_2(g) + RC(O)O^-(g) \rightarrow RC(O)OI(g) + I^-(g) \quad (8a)$$

$$HOI(g) + RC(O)O^-(g) \rightarrow RC(O)OI(g) + OH^-(g) \quad (8b)$$

$RC(O)O^-$ is generated by the reaction of RCOOH with O_2^- (Figure S2 of the Supporting Information) upon PDG ionization and is proposed to react with RC(O)OI to form the $[2M - 2H + I]^-$ adduct in the gas phase via reaction 9.

$$RC(O)O^-(g) + RC(O)OI(g) \rightarrow [RC(O)OI\cdots O(O)CR]^-(g) \quad (9)$$

DOI: 10.1021/acsearthspacechem.9b00030
ACS Earth Space Chem. 2019, 3, 1315−1328

The apparent stability of these unusual $[2M - 2H + I]^-$ clusters may be reconciled through halogen bonds. Acyl hypoiodites are known to possess a larger σ hole on the extension of the O–I axis, as shown in Figure 7, than

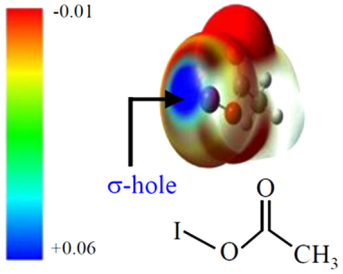

Figure 7. Electrostatic potential diagram showing the σ hole in acetyl hypoiodite on the same scale as Figure 1. This figure was adapted with permission from ref 91. Copyright 2018 John Wiley & Sons, Inc.

molecular iodine has on the extension of the I–I axis (Figure 1).[91] The strength of the halogen bond interaction increases with the size of the σ hole. We propose that an attractive noncovalent interaction between the electrophilic region of the iodine atom in RC(O)OI and the nucleophilic carboxylate anion, $RC(O)O^-$, the Lewis base, may account for the $[2M - 2H + I]^-$ clusters.

Further evidence that reactions 8 and 9 occur in the gas phase is provided by experiments in which the C_5 and C_6 acid liquids were held in two separate capillaries and ionized alongside the capillary containing iodine tincture with the PDG. Mass spectra from this experiment show the C_5 $[2M_5 - 2H + I]^-$ cluster, the C_6 $[2M_6 - 2H + I]^-$ cluster, and a mixed C_5/C_6 $[M_5 + M_6 - 2H + I]^-$ cluster, as shown in Figure 8.

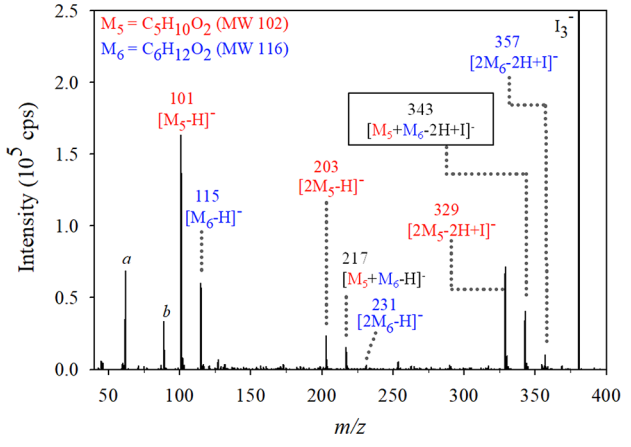

Figure 8. Mass spectrum obtained from PDG ionization of the iodine tincture and pentanoic and hexanoic acids each in separate capillaries showing the formation of a mixed C_5/C_6 $[M_5 + M_6 - 2H + I]^-$ cluster at m/z 343. Peaks labeled *a* and *b* at m/z 62 and 89, respectively, are due to NO_3^- and lactic acid $[M - H]^-$.

Because the liquid analytes are in separate capillaries and are not in contact with each other, a mixed cluster can only form if the C_5 and C_6 acids evaporate before they are ionized by PDG. The presence of the mixed C_5/C_6 cluster upon ionization of each acid held in separate capillaries therefore confirms that the $[2M - 2H + I]^-$ ions form in the vapor phase. As seen in Figure 9, MS/MS experiments again show the expected product ions $[M - H]^-$ for C_5 and C_6 acids, which correspond to the neutral loss of RC(O)OI.

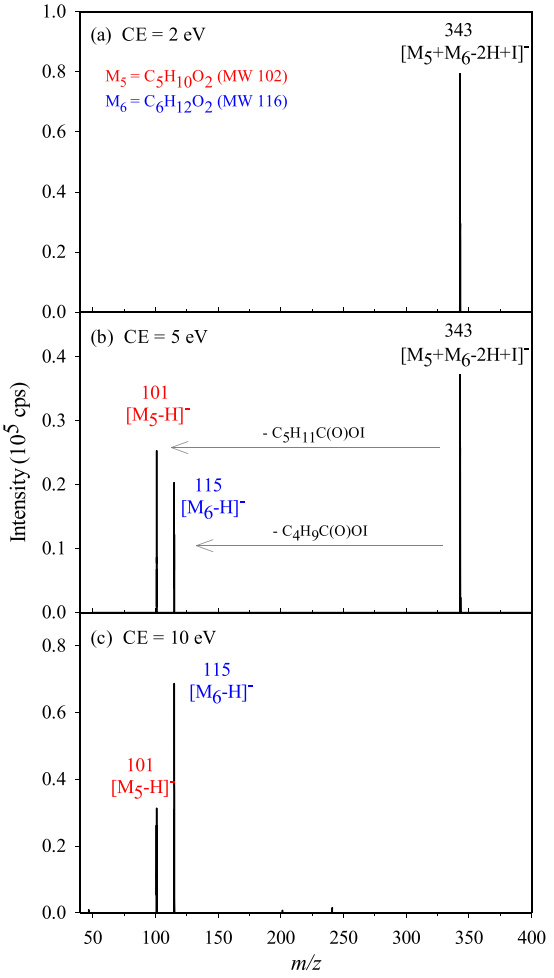

Figure 9. Product ion scans of the m/z 343 $[M_5 + M_6 - 2H + I]^-$ cluster identified in Figure 8 at collision energies of (a) 2 eV, (b) 5 eV, and (c) 10 eV.

A competitive interaction will exist between hydrogen bond and halogen bond formation in the detected $[2M - H]^-$ and $[2M - 2H + I]^-$ adducts. Thus, in competition with reaction 9, $RC(O)O^-$ may come into contact with undissociated RCOOH molecules in the vapor phase, leading to $[2M - H]^-$ adducts (reaction 10).

$$RC(O)O^-(g) + RC(O)OH(g) \rightarrow [RC(O)O\cdots HO(O)CR]^-(g) \quad (10)$$

For both formic and acetic acids, the $[2M - H]^-$ ion is more intense than the $[2M - 2H + I]^-$ cluster (Figure 6). As the carbon chain length increases, there is a preference to form halogen-bonded $[2M - 2H + I]^-$ over the hydrogen-bonded adduct, $[2M - H]^-$. This trend is shown in Figure 10, in which the $[2M - H]^-/[2M - 2H + I]^-$ peak intensity ratio is provided for each of the C_1–C_9 monocarboxylic acids. The stability of the longer chain clusters $[2M - 2H + I]^-$ may be due to a larger number of accessible vibrational modes, which allow excess energy to be redistributed.

As the carbon chain lengthens in the homologous acid series, the positive inductive effect of the aliphatic chain of the acyl

DOI: 10.1021/acsearthspacechem.9b00030
ACS Earth Space Chem. 2019, 3, 1315–1328

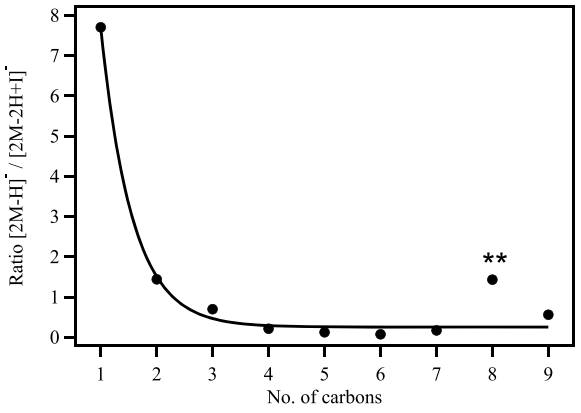

Figure 10. Ratio of $[2M - H]^-$ to $[2M - 2H + I]^-$ peak intensities for C_1–C_9 alkanoic acids ionized by PDG with the iodine tincture. The curve is a guide for the eye only. The presence of $(HOI)OI^-$ ion at m/z 287 (**) interferes with the $[2M - H]^-$ ion for C_8.

hypoiodite is expected to increase. Although it would seem that this would reduce the electrophilicity of the iodine atom, thereby decreasing the size of the σ hole, instead, the longer chains appear to stabilize the halogen bond. This counter-intuitive trend was noted in a density functional theory (DFT) study of C_1–C_5 acyl hypoiodites interacting with substituted pyridine bases[91] and other halogen bond studies.[121,122] Guha and Sekar[91] report that the increasing positive inductive effect across the acyl hypoiodite series lowers the lowest unoccupied molecular orbital (LUMO) acceptor orbital energies relative to the energy of the highest occupied molecular orbital (HOMO) donor orbital, resulting in a significant mixing of the frontier orbitals. In addition, the nucleophilicity of $RCOO^-$ increases as its carbon chain lengthens, increasing its attraction to the σ hole. Thus, increasing the carbon chain length on both reactants in reaction 9 acts to stabilize $[2M - 2H + I]^-$ adduct formation.

To gain further insight into the formation mechanism for $[2M - 2H + I]^-$ clusters, each of the acids were ionized with the PDG ionization technique using CH_3I as the reagent ion source instead of the I_2 tincture. None of the acids formed the $[2M - 2H + I]^-$ clusters, and only the $[M - H]^-$ ion was consistently observed. Examples are shown in panels b–d of Figure S6 of the Supporting Information for acetic, hexanoic, and octanoic acids. This result lends strong support for reactions of HOI and its clusters with $RCOO^-$ as the origin of acyl hypoiodite in the I_2 tincture spectra.

Applications to Other Carboxylic Acids. Carboxylic acids having structural features not found in the alkanoic acid series were studied to ascertain whether the $[2M - 2H + I]^-$ cluster would form. Specifically, benzoic acid (Figure 11a), observed in indoor air,[123] and 2,2-dimethylpropanoic acid (Figure 11b), emitted from building materials,[124,125] both formed the $[2M - 2H + I]^-$ cluster. In addition, a monounsaturated acid, 9-decenoic acid, found in the headspace of wine[126] and other foods[127−132] also forms the $[2M - 2H + I]^-$ cluster (Figure 11c). These data demonstrate that both alkyl and aryl carboxylic acids lead to gas-phase RCOOI formation, followed by halogen bond formation with their $RCOO^-$ counterparts. Aryl (Ar) hypoidoites are known to interact with carboxylate ions through non-covalent inter-

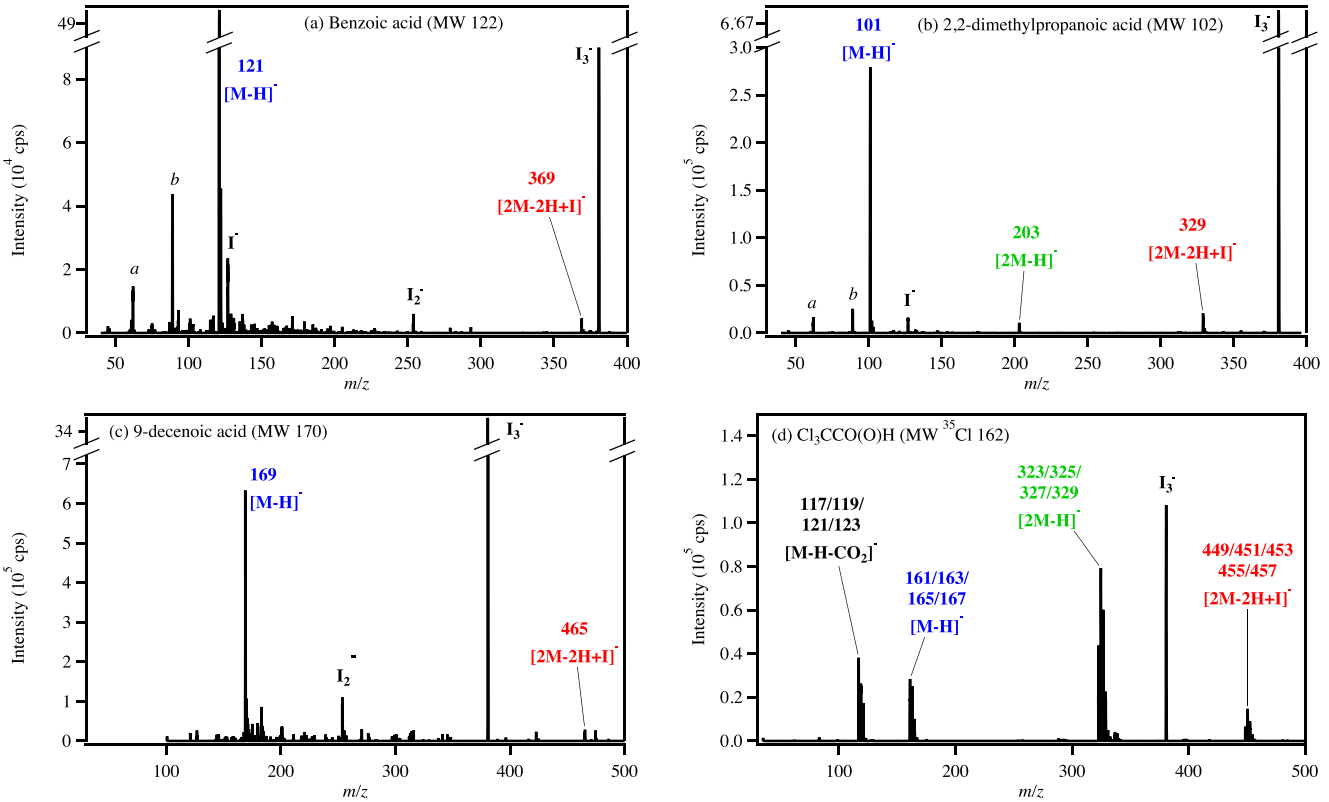

Figure 11. Mass spectra obtained from PDG ionization with the iodine tincture of (a) benzoic acid, (b) 2,2-dimethylpropanoic acid, (c) 9-decenoic acid, and (d) trichloroacetic acid. In panel d, the molecular weight of only the ^{35}Cl isotopomer is provided but the analyte contained the natural abundances of all isotopomers. Peaks labeled *a* and *b* at m/z 62 and 89, respectively, are due to NO_3^- and lactic acid $[M - H]^-$.

DOI: 10.1021/acsearthspacechem.9b00030
ACS Earth Space Chem. 2019, 3, 1315−1328

actions to form ions of the type $[Ar{-}C(O)OI{\cdots}O(O)C{-}Ar]^-$.[133]

Finally, trichloroacetic acid (Figure 11d), which has been measured in air[134,135] and water,[136] shows the $[2M - 2H + I]^-$ peak and also gives rise to a $[M - H - CO_2]^-$ peak, characteristic of trihaloacetic acids.[137] The presence of the $[2M - 2H + I]^-$ peak speaks to the negative inductive effect provided by the chlorine substituents, which render iodine in the corresponding trichloroacetyl hypoiodite more positive.[138,139] In short, the $[2M - 2H + I]^-$ cluster forms consistently for a variety of carboxylic acids with a range of structural features.

The formation of gaseous acyl hypoiodite ion clusters, $[2M - 2H + I]^-$, is the first direct evidence for halogen bonding in plasma-induced ionization in the gas phase. Given the importance of halogen chemistry in the troposphere,[76,78,140,141] the question arises as to whether halogen bonding may play a role in chemical processes in the atmosphere. Halogen-bonded complexes between CH_3I and CCl_4 with oxygenated organics[142] have been observed, and theoretical studies of HOI binding to dimethyl sulfoxide[113] and monohaloamines[143] predict halogen bonding in those cases as well. There is also evidence for halogen bonding of water with HOX (X = F, Cl, and Br)[144] and with CF_4 and CCl_4.[145] Of these possibilities in the atmosphere, only water is likely to be present in sufficient concentrations to complex significantly in the gas phase under atmospheric conditions, potentially affecting the reactivity of the halogen compound.

However, halogen bonding may play a more important role in the condensed phase found in particles. Yu et al.[146] reported the presence of a number of organic iodine compounds in particles in China under conditions where new particle formation was occurring. They proposed formation via electrophilic substitutions involving I^+ formed from HOI or I_2. However, it might be that the formation of these organoiodine compounds actually proceeds via halogen bonds rather than I^+. Thus, the contribution of halogen bonds, especially for HOI and other iodine-containing species, warrants further investigation in the condensed-phase chemistry of the marine boundary layer.

CONCLUSION

A hand-held PDG combined with a commercial iodine tincture was shown to generate a suite of ions during ambient ionization with the detected adducts, with strong evidence for halogen bonding. The technique is shown to detect the molecular halogens, Cl_2 and Br_2, as well as nitric and organic acids. For the acids, secondary chemistry occurs involving hypoiodite to generate $[2M - 2H + I]^-$ cluster ions, which are stabilized through halogen bonding between acyl hypoiodites and the deprotonated acids. This chemistry is analogous to the reaction of HOI with NO_3^- to form $IONO_2$. The formation of $[2M - 2H + I]^-$ cluster ions is the first direct evidence for halogen bonding in the gas phase following plasma-induced ionization.

The observations of halogen bonds with the atmospherically relevant species in these studies suggest that this bonding may play a role in the troposphere. While the importance of halogen bonding in the troposphere is likely to be limited to iodine species interacting with water vapor as a result of the high concentrations of the latter, halogen bonding may be important in the condensed particle phase in which organic iodine compounds have been implicated in new particle formation.

ASSOCIATED CONTENT

Supporting Information

The Supporting Information is available free of charge on the ACS Publications website at DOI: 10.1021/acsearthspacechem.9b00030.

Time resolution and influence of the instrument scanning rate (Figure S1), proposed mechanisms for PDG ambient ionization (Figure S2), UV/vis spectra of liquid iodine tincture (Figure S3), negative ion mode mass spectra of I_2 tincture using PDG and DART ionization (Figure S4), product ion scans of HOI and OI^- adducts (Figure S5), mass spectra generated using PDG ionization of CH_3I with and without carboxylic reagents (Figure S6), negative ion mode DART mass spectra of I_2 tincture in the absence and prescence of HNO_3 (Figure S7), product ion scans of the $[2M - 2H + I]^-$ clusters formed from PDG ionization with the I_2 tincture for acetic and nonanoic acids (Figure S8), and thermodynamic data of relevant species (Table S1) (PDF)

AUTHOR INFORMATION

Corresponding Author

*Telephone: 310-506-4054. E-mail: jane.ganske@pepperdine.edu.

ORCID

Jane A. Ganske: 0000-0002-0273-0862
Lisa M. Wingen: 0000-0001-5847-9913
Véronique Perraud: 0000-0003-1247-9787
Barbara J. Finlayson-Pitts: 0000-0003-4650-168X

Notes

The authors declare no competing financial interest.

ACKNOWLEDGMENTS

The authors are grateful to the Army Research Office (Grant W911NF1710105), the National Science Foundation (NSF, Grant 1647386), and the NSF Major Research Instrumentation (MRI) program (Grant 1337080) for support of this work. Jane A. Ganske was supported by a Seaver Dean's Research grant from Pepperdine University. The authors thank Professors Christopher Vanderwal, Donald Blake, John Hemminger, and Saewung Kim for providing some chemicals and Michael Ezell for helpful discussions. The authors also thank Victor Griganavicius, Michael Gabriel, and Bryan Humphries (Waters) for mass spectrometer support. Finally, the authors thank the two anonymous reviewers for insightful comments.

REFERENCES

(1) Huey, L. G. Measurement of trace atmospheric species by chemical ionization mass spectrometry: Speciation of reactive nitrogen and future directions. *Mass Spectrom. Rev.* **2007**, *26*, 166–184.

(2) Cooks, R. G.; Jarmusch, A. K.; Wleklinski, M. Direct analysis of complex mixtures by mass spectrometry. *Int. J. Mass Spectrom.* **2015**, *377*, 709–718.

(3) Laskin, J.; Laskin, A.; Nizkorodov, S. A. Mass spectrometry analysis in atmospheric chemistry. *Anal. Chem.* **2018**, *90* (1), 166–189.

DOI: 10.1021/acsearthspacechem.9b00030
ACS Earth Space Chem. 2019, 3, 1315–1328

(4) Aljawhary, D.; Lee, A. K. Y.; Abbatt, J. P. D. High-resolution chemical ionization mass spectrometry (ToF-CIMS): Application to study SOA composition and processing. *Atmos. Meas. Tech.* **2013**, *6* (11), 3211−3224.
(5) Francis, G. J.; Langford, V. S.; Milligan, D. B.; McEwan, M. J. Real-time monitoring of hazardous air pollutants. *Anal. Chem.* **2009**, *81* (4), 1595−1599.
(6) Hearn, J. D.; Smith, G. D. A chemical ionization mass spectrometry method for the online analysis of organic aerosols. *Anal. Chem.* **2004**, *76* (10), 2820−2826.
(7) Wang, Y.; Hua, L.; Li, Q.; Jiang, J.; Hou, K.; Wu, C.; Li, H. Direct detection of small n-alkanes at sub-ppbv level by photoelectron-induced O_2^+ cation chemical ionization mass spectrometry at kPa pressure. *Anal. Chem.* **2018**, *90* (8), 5398−5404.
(8) Yao, L.; Wang, M. Y.; Wang, X. K.; Liu, Y. J.; Chen, H. F.; Zheng, J.; Nie, W.; Ding, A. J.; Geng, F. H.; Wang, D. F.; Chen, J. M.; Worsnop, D. R.; Wang, L. Detection of atmospheric gaseous amines and amides by a high-resolution time-of-flight chemical ionization mass spectrometer with protonated ethanol reagent ions. *Atmos. Chem. Phys.* **2016**, *16* (22), 14527−14543.
(9) You, Y.; Kanawade, V. P.; de Gouw, J. A.; Guenther, A. B.; Madronich, S.; Sierra-Hernandez, M. R.; Lawler, M.; Smith, J. N.; Takahama, S.; Ruggeri, G.; Koss, A.; Olson, K.; Baumann, K.; Weber, R. J.; Nenes, A.; Guo, H.; Edgerton, E. S.; Porcelli, L.; Brune, W. H.; Goldstein, A. H.; Lee, S. H. Atmospheric amines and ammonia measured with a chemical ionization mass spectrometer (CIMS). *Atmos. Chem. Phys.* **2014**, *14* (22), 12181−12194.
(10) Yu, H.; Lee, S. H. Chemical ionisation mass spectrometry for the measurement of atmospheric amines. *Environ. Chem.* **2012**, *9* (3), 190−201.
(11) Berresheim, H.; Elste, T.; Plass-Dulmer, C.; Eisele, F. L.; Tanner, D. J. Chemical ionization mass spectrometer for long-term measurements of atmospheric OH and H_2SO_4. *Int. J. Mass Spectrom.* **2000**, *202* (1−3), 91−109.
(12) Jokinen, T.; Sipila, M.; Junninen, H.; Ehn, M.; Lonn, G.; Hakala, J.; Petaja, T.; Mauldin, R. L.; Kulmala, M.; Worsnop, D. R. Atmospheric sulphuric acid and neutral cluster measurements using CI-APi-TOF. *Atmos. Chem. Phys.* **2012**, *12* (9), 4117−4125.
(13) Ehn, M.; Thornton, J. A.; Kleist, E.; Sipila, M.; Junninen, H.; Pullinen, I.; Springer, M.; Rubach, F.; Tillmann, R.; Lee, B.; Lopez-Hilfiker, F.; Andres, S.; Acir, I. H.; Rissanen, M.; Jokinen, T.; Schobesberger, S.; Kangasluoma, J.; Kontkanen, J.; Nieminen, T.; Kurten, T.; Nielsen, L. B.; Jorgensen, S.; Kjaergaard, H. G.; Canagaratna, M.; Dal Maso, M.; Berndt, T.; Petaja, T.; Wahner, A.; Kerminen, V. M.; Kulmala, M.; Worsnop, D. R.; Wildt, J.; Mentel, T. F. A large source of low-volatility secondary organic aerosol. *Nature* **2014**, *506* (7489), 476−479.
(14) Massoli, P.; Stark, H.; Canagaratna, M. R.; Krechmer, J. E.; Xu, L.; Ng, N. L.; Mauldin, R. L.; Yan, C.; Kimmel, J.; Misztal, P. K.; Jimenez, J. L.; Jayne, J. T.; Worsnop, D. R. Ambient measurements of highly oxidized gas-phase molecules during the Southern Oxidant and Aerosol Study (SOAS) 2013. *ACS Earth Space Chem.* **2018**, *2* (7), 653−672.
(15) Crounse, J. D.; McKinney, K. A.; Kwan, A. J.; Wennberg, P. O. Measurement of gas-phase hydroperoxides by chemical ionization mass spectrometry. *Anal. Chem.* **2006**, *78* (19), 6726−6732.
(16) Beaver, M. R.; St. Clair, J. M.; Paulot, F.; Spencer, K. M.; Crounse, J. D.; LaFranchi, B. W.; Min, K. E.; Pusede, S. E.; Wooldridge, P. J.; Schade, G. W.; Park, C.; Cohen, R. C.; Wennberg, P. O. Importance of biogenic precursors to the budget of organic nitrates: Observations of multifunctional organic nitrates by CIMS and TD-LIF during BEARPEX 2009. *Atmos. Chem. Phys.* **2012**, *12* (13), 5773−5785.
(17) Huey, L. G.; Tanner, D. J.; Slusher, D. L.; Dibb, J. E.; Arimoto, R.; Chen, G.; Davis, D.; Buhr, M. P.; Nowak, J. B.; Mauldin, R. L.; Eisele, F. L.; Kosciuch, E. CIMS measurements of HNO_3 and SO_2 at the south pole during ISCAT 2000. *Atmos. Environ.* **2004**, *38* (32), 5411−5421.
(18) Huey, L. G.; Hanson, D. R.; Howard, C. J. Reactions of SF_6^- and I^- with atmospheric trace gases. *J. Phys. Chem.* **1995**, *99* (14), 5001−5008.
(19) Nah, T.; Ji, Y.; Tanner, D. J.; Guo, H. Y.; Sullivan, A. P.; Ng, N. L.; Weber, R. J.; Huey, L. G. Real-time measurements of gas-phase organic acids using SF_6^- chemical ionization mass spectrometry. *Atmos. Meas. Tech.* **2018**, *11* (9), 5087−5104.
(20) Veres, P.; Roberts, J. M.; Burling, I. R.; Warneke, C.; de Gouw, J.; Yokelson, R. J. Measurements of gas-phase inorganic and organic acids from biomass fires by negative-ion proton-transfer chemical-ionization mass spectrometry. *J. Geophys. Res.* **2010**, *115*, D23302.
(21) Veres, P.; Roberts, J. M.; Warneke, C.; Welsh-Bon, D.; Zahniser, M.; Herndon, S.; Fall, R.; de Gouw, J. Development of negative-ion proton-transfer chemical-ionization mass spectrometry (NI-PT-CIMS) for the measurement of gas-phase organic acids in the atmosphere. *Int. J. Mass Spectrom.* **2008**, *274* (1−3), 48−55.
(22) Bertram, T. H.; Kimmel, J. R.; Crisp, T. A.; Ryder, O. S.; Yatavelli, R. L. N.; Thornton, J. A.; Cubison, M. J.; Gonin, M.; Worsnop, D. R. A field-deployable, chemical ionization time-of-flight mass spectrometer. *Atmos. Meas. Tech.* **2011**, *4* (7), 1471−1479.
(23) Arijs, E.; Barassin, A.; Kopp, E.; Amelynck, C.; Catoire, V.; Fink, H. P.; Guimbaud, C.; Jenzer, U.; Labonnette, D.; Luithardt, W.; Neefs, E.; Nevejans, D.; Schoon, N.; Van Bavel, A. M. Stratospheric chemical ionization mass spectrometry: Nitric acid detection by different ion molecule reaction schemes. *Int. J. Mass Spectrom.* **1998**, *181*, 99−111.
(24) Huey, L. G.; Lovejoy, E. R. Reactions of SiF_5^- with atmospheric trace gases: Ion chemistry for chemical ionization detection of HNO_3 in the troposphere. *Int. J. Mass Spectrom. Ion Processes* **1996**, *155* (3), 133−140.
(25) Hanson, D. R.; Ravishankara, A. R. The reaction probabilities of $ClONO_2$ and N_2O_5 on polar stratospheric cloud materials. *J. Geophys. Res.* **1991**, *96* (D3), 5081−5090.
(26) McNeill, V. F.; Wolfe, G. M.; Thornton, J. A. The oxidation of oleate in submicron aqueous salt aerosols: Evidence of a surface process. *J. Phys. Chem. A* **2007**, *111* (6), 1073−1083.
(27) Kercher, J. P.; Riedel, T. P.; Thornton, J. A. Chlorine activation by N_2O_5: Simultaneous, in situ detection of $ClNO_2$ and N_2O_5 by chemical ionization mass spectrometry. *Atmos. Meas. Tech.* **2009**, *2* (1), 193−204.
(28) Iyer, S.; He, X. C.; Hyttinen, N.; Kurten, T.; Rissanen, M. P. Computational and experimental investigation of the detection of HO_2 radical and the products of its reaction with cyclohexene ozonolysis derived RO_2 radicals by an iodide-based chemical ionization mass spectrometer. *J. Phys. Chem. A* **2017**, *121* (36), 6778−6789.
(29) Iyer, S.; Lopez-Hilfiker, F.; Lee, B. H.; Thornton, J. A.; Kurten, T. Modeling the detection of organic and inorganic compounds using iodide-based chemical ionization. *J. Phys. Chem. A* **2016**, *120* (4), 576−587.
(30) Lee, B. H.; Lopez-Hilfiker, F. D.; Mohr, C.; Kurten, T.; Worsnop, D. R.; Thornton, J. A. An iodide-adduct high-resolution time-of-flight chemical-ionization mass spectrometer: Application to atmospheric inorganic and organic compounds. *Environ. Sci. Technol.* **2014**, *48* (11), 6309−6317.
(31) Hyttinen, N.; Otkjaer, R. V.; Iyer, S.; Kjaergaard, H. G.; Rissanen, M. P.; Wennberg, P. O.; Kurten, T. Computational comparison of different reagent ions in the chemical ionization of oxidized multifunctional compounds. *J. Phys. Chem. A* **2018**, *122* (1), 269−279.
(32) Eger, P. G.; Helleis, F.; Schuster, G.; Phillips, G. J.; Lelieveld, J.; Crowley, J. N. Chemical ionisation quadrupole mass spectrometer with an electrical discharge ion source for atmospheric trace gas measurement. *Atmos. Meas. Technol. Discuss.* **2018**, *2018*, 1−35.
(33) Custard, K. D.; Raso, A. R. W.; Shepson, P. B.; Staebler, R. M.; Pratt, K. A. Production and release of molecular bromine and chlorine from the arctic coastal snowpack. *ACS Earth Space Chem.* **2017**, *1* (3), 142−151.

DOI: 10.1021/acsearthspacechem.9b00030
ACS Earth Space Chem. 2019, 3, 1315−1328

(34) Lee, B. H.; Lopez-Hilfiker, F. D.; Schroder, J. C.; Campuzano-Jost, P.; Jimenez, J. L.; McDuffie, E. E.; Fibiger, D. L.; Veres, P. R.; Brown, S. S.; Campos, T. L.; Weinheimer, A. J.; Flocke, F. F.; Norris, G.; O'Mara, K.; Green, J. R.; Fiddler, M. N.; Bililign, S.; Shah, V.; Jaeglé, L.; Thornton, J. A. Airborne observations of reactive inorganic chlorine and bromine species in the exhaust of coal-fired power plants. *J. Geophys. Res.: Atmos.* **2018**, *123* (19), 11,225−11,237.
(35) Lee, B. H.; Lopez-Hilfiker, F. D.; Veres, P. R.; McDuffie, E. E.; Fibiger, D. L.; Sparks, T. L.; Ebben, C. J.; Green, J. R.; Schroder, J. C.; Campuzano-Jost, P.; Iyer, S.; D'Ambro, E. L.; Schobesberger, S.; Brown, S. S.; Wooldridge, P. J.; Cohen, R. C.; Fiddler, M. N.; Bililign, S.; Jimenez, J. L.; Kurtén, T.; Weinheimer, A. J.; Jaegle, L.; Thornton, J. A. Flight deployment of a high-resolution time-of-flight chemical ionization mass spectrometer: Observations of reactive halogen and nitrogen oxide species. *J. Geophys. Res.: Atmos.* **2018**, *123* (14), 7670−7686.
(36) Liao, J.; Huey, L. G.; Liu, Z.; Tanner, D. J.; Cantrell, C. A.; Orlando, J. J.; Flocke, F. M.; Shepson, P. B.; Weinheimer, A. J.; Hall, S. R.; Ullmann, K.; Beine, H. J.; Wang, Y. H.; Ingall, E. D.; Stephens, C. R.; Hornbrook, R. S.; Apel, E. C.; Riemer, D.; Fried, A.; Mauldin, R. L.; Smith, J. N.; Staebler, R. M.; Neuman, J. A.; Nowak, J. B. High levels of molecular chlorine in the Arctic atmosphere. *Nat. Geosci.* **2014**, *7* (2), 91−94.
(37) Liao, J.; Huey, L. G.; Tanner, D. J.; Flocke, F. M.; Orlando, J. J.; Neuman, J. A.; Nowak, J. B.; Weinheimer, A. J.; Hall, S. R.; Smith, J. N.; Fried, A.; Staebler, R. M.; Wang, Y.; Koo, J. H.; Cantrell, C. A.; Weibring, P.; Walega, J.; Knapp, D. J.; Shepson, P. B.; Stephens, C. R. Observations of inorganic bromine (HOBr, BrO, and Br_2) speciation at Barrow, Alaska, in spring 2009. *J. Geophys. Res.: Atmos.* **2012**, *117*, 11.
(38) Raso, A. R. W.; Custard, K. D.; May, N. W.; Tanner, D.; Newburn, M. K.; Walker, L.; Moore, R. J.; Huey, L. G.; Alexander, L.; Shepson, P. B.; Pratt, K. A. Active molecular iodine photochemistry in the Arctic. *Proc. Natl. Acad. Sci. U. S. A.* **2017**, *114* (38), 10053−10058.
(39) Riedel, T. P.; Bertram, T. H.; Ryder, O. S.; Liu, S.; Day, D. A.; Russell, L. M.; Gaston, C. J.; Prather, K. A.; Thornton, J. A. Direct N_2O_5 reactivity measurements at a polluted coastal site. *Atmos. Chem. Phys.* **2012**, *12* (6), 2959−2968.
(40) Custard, K. D.; Pratt, K. A.; Wang, S.; Shepson, P. B. Constraints on arctic atmospheric chlorine production through measurements and simulations of Cl_2 and ClO. *Environ. Sci. Technol.* **2016**, *50* (22), 12394−12400.
(41) Slusher, D. L.; Huey, L. G.; Tanner, D. J.; Flocke, F. M.; Roberts, J. M. A thermal dissociation−chemical ionization mass spectrometry (TD-CIMS) technique for the simultaneous measurement of peroxyacyl nitrates and dinitrogen pentoxide. *J. Geophys. Res.: Atmos.* **2004**, *109* (D19), D19315.
(42) Crowley, J. N.; Pouvesle, N.; Phillips, G. J.; Axinte, R.; Fischer, H.; Petaja, T.; Nolscher, A.; Williams, J.; Hens, K.; Harder, H.; Martinez-Harder, M.; Novelli, A.; Kubistin, D.; Bohn, B.; Lelieveld, J. Insights into HO_x and RO_x chemistry in the boreal forest via measurement of peroxyacetic acid, peroxyacetic nitric anhydride (PAN) and hydrogen peroxide. *Atmos. Chem. Phys.* **2018**, *18* (18), 13457−13479.
(43) Neuman, J. A.; Trainer, M.; Brown, S. S.; Min, K. E.; Nowak, J. B.; Parrish, D. D.; Peischl, J.; Pollack, I. B.; Roberts, J. M.; Ryerson, T. B.; Veres, P. R. HONO emission and production determined from airborne measurements over the southeast US. *J. Geophys. Res.: Atmos.* **2016**, *121* (15), 9237−9250.
(44) Lopez-Hilfiker, F. D.; Iyer, S.; Mohr, C.; Lee, B. H.; D'Ambro, E. L.; Kurten, T.; Thornton, J. A. Constraining the sensitivity of iodide adduct chemical ionization mass spectrometry to multifunctional organic molecules using the collision limit and thermodynamic stability of iodide ion adducts. *Atmos. Meas. Tech.* **2016**, *9* (4), 1505−1512.
(45) Phillips, G. J.; Tang, M. J.; Thieser, J.; Brickwedde, B.; Schuster, G.; Bohn, B.; Lelieveld, J.; Crowley, J. N. Significant concentrations of nitryl chloride observed in rural continental Europe associated with the influence of sea salt chloride and anthropogenic emissions. *Geophys. Res. Lett.* **2012**, *39*, L10811.
(46) Phillips, G. J.; Pouvesle, N.; Thieser, J.; Schuster, G.; Axinte, R.; Fischer, H.; Williams, J.; Lelieveld, J.; Crowley, J. N. Peroxyacetyl nitrate (PAN) and peroxyacetic acid (PAA) measurements by iodide chemical ionisation mass spectrometry: First analysis of results in the boreal forest and implications for the measurement of PAN fluxes. *Atmos. Chem. Phys.* **2013**, *13* (3), 1129−1139.
(47) Wang, X. F.; Wang, T.; Xue, L. K.; Nie, W.; Xu, Z.; Poon, S. C. N.; Wang, W. X. Peroxyacetyl nitrate measurements by thermal dissociation−chemical ionization mass spectrometry in an urban environment: Performance and characterizations. *Front. Environ. Sci. Eng.* **2017**, *11* (4), 3.
(48) Cooks, R. G.; Ouyang, Z.; Takats, Z.; Wiseman, J. M. Ambient mass spectrometry. *Science* **2006**, *311* (5767), 1566−1570.
(49) Laskin, A.; Laskin, J.; Nizkorodov, S. A. Mass spectrometric approaches for chemical characterisation of atmospheric aerosols: Critical review of the most recent advances. *Environ. Chem.* **2012**, *9* (3), 163−189.
(50) Laskin, J.; Laskin, A.; Nizkorodov, S. A. New mass spectrometry techniques for studying physical chemistry of atmospheric heterogeneous processes. *Int. Rev. Phys. Chem.* **2013**, *32* (1), 128−170.
(51) Domin, M.; Cody, R. *Ambient Ionization Mass Spectrometry*; Royal Society of Chemistry: London, U.K., 2015.
(52) Feider, C. L.; Krieger, A.; DeHoog, R. J.; Eberlin, L. S. Ambient Ionization Mass Spectrometry: Recent Developments and Applications. *Anal. Chem.* **2019**, *91* (7), 4266−4290.
(53) Zhao, Y.; Fairhurst, M. C.; Wingen, L. M.; Perraud, V.; Ezell, M. J.; Finlayson-Pitts, B. J. New insights into atmospherically relevant reaction systems using direct analysis in real-time mass spectrometry (DART-MS). *Atmos. Meas. Tech.* **2017**, *10* (4), 1373−1386.
(54) Kumbhani, S.; Longin, T.; Wingen, L. M.; Kidd, C.; Perraud, V.; Finlayson-Pitts, B. J. New mechanism of extractive electrospray ionization mass spectrometry for heterogeneous solid particles. *Anal. Chem.* **2018**, *90* (3), 2055−2062.
(55) Wingen, L. M.; Finlayson-Pitts, B. J. Probing surfaces of atmospherically relevant organic particles by easy ambient sonic-spray ionization mass spectrometry (EASI-MS). *Chem. Sci.* **2019**, *10* (3), 884−897.
(56) Chan, M. N.; Nah, T.; Wilson, K. R. Real time in situ chemical characterization of sub-micron organic aerosols using Direct Analysis in Real Time mass spectrometry (DART-MS): The effect of aerosol size and volatility. *Analyst* **2013**, *138* (13), 3749−3757.
(57) Nah, T.; Chan, M.; Leone, S. R.; Wilson, K. R. Real time in situ chemical characterization of submicrometer organic particles using direct analysis in real time-mass spectrometry. *Anal. Chem.* **2013**, *85* (4), 2087−2095.
(58) Gallimore, P. J.; Kalberer, M. Characterizing an extractive electrospray ionization (EESI) source for the online mass spectrometry analysis of organic aerosols. *Environ. Sci. Technol.* **2013**, *47* (13), 7324−7331.
(59) Law, W. S.; Chen, H. W.; Balabin, R.; Berchtold, C.; Meier, L.; Zenobi, R. Rapid fingerprinting and classification of extra virgin olive oil by microjet sampling and extractive electrospray ionization mass spectrometry. *Analyst* **2010**, *135* (4), 773−778.
(60) Kumbhani, S. R.; Wingen, L. M.; Perraud, V.; Finlayson-Pitts, B. J. A cautionary note on the effects of laboratory air contaminants on ambient ionization mass spectrometry measurements. *Rapid Commun. Mass Spectrom.* **2017**, *31* (19), 1659−1668.
(61) Horan, A. J.; Gao, Y.; Hall, W. A.; Johnston, M. V. Online characterization of particles and gases with an ambient electrospray ionization source. *Anal. Chem.* **2012**, *84* (21), 9253−9258.
(62) Chen, H. W.; Zenobi, R. Neutral desorption sampling of biological surfaces for rapid chemical characterization by extractive electrospray ionization mass spectrometry. *Nat. Protoc.* **2008**, *3* (9), 1467−1475.
(63) Chingin, K.; Gamez, G.; Chen, H. W.; Zhu, L.; Zenobi, R. Rapid classification of perfumes by extractive electrospray ionization

DOI: 10.1021/acsearthspacechem.9b00030
ACS Earth Space Chem. 2019, 3, 1315−1328

mass spectrometry (EESI-MS). *Rapid Commun. Mass Spectrom.* **2008**, *22* (13), 2009−2014.
(64) Ding, J. H.; Yang, S. P.; Liang, D. P.; Chen, H. W.; Wu, Z. Z.; Zhang, L. L.; Ren, Y. L. Development of extractive electrospray ionization ion trap mass spectrometry for in vivo breath analysis. *Analyst* **2009**, *134* (10), 2040−2050.
(65) Meier, L.; Schmid, S.; Berchtold, C.; Zenobi, R. Contribution of liquid-phase and gas-phase ionization in extractive electrospray ionization mass spectrometry of primary amines. *Eur. J. Mass Spectrom.* **2011**, *17* (4), 345−351.
(66) Zhu, L. A.; Hu, Z.; Gamez, G.; Law, W. S.; Chen, H. W.; Yang, S. P.; Chingin, K.; Balabin, R. M.; Wang, R.; Zhang, T. T.; Zenobi, R. Simultaneous sampling of volatile and non-volatile analytes in beer for fast fingerprinting by extractive electrospray ionization mass spectrometry. *Anal. Bioanal. Chem.* **2010**, *398* (1), 405−413.
(67) Campbell, D. I.; Dalgleish, J. K.; Cotte-Rodriguez, I.; Maeno, S.; Graham Cooks, R. Chemical analysis and chemical imaging of fragrances and volatile compounds by low-temperature plasma ionization mass spectrometry. *Rapid Commun. Mass Spectrom.* **2013**, *27* (16), 1828−1836.
(68) Dalgleish, J. K.; Hou, K.; Ouyang, Z.; Cooks, R. G. In situ explosive detection using a miniature plasma ion source and a portable mass spectrometer. *Anal. Lett.* **2012**, *45* (11), 1440−1446.
(69) Harper, J. D.; Charipar, N. A.; Mulligan, C. C.; Zhang, X.; Cooks, R. G.; Ouyang, Z. Low-temperature plasma probe for ambient desorption ionization. *Anal. Chem.* **2008**, *80* (23), 9097−9104.
(70) Wiley, J. S.; Shelley, J. T.; Cooks, R. G. Handheld Low-Temperature Plasma Probe for Portable "Point-and-Shoot" Ambient Ionization Mass Spectrometry. *Anal. Chem.* **2013**, *85* (14), 6545−6552.
(71) Li, A. Y.; Hollerbach, A.; Luo, Q. J.; Cooks, R. G. On-demand ambient ionization of picoliter samples using charge pulses. *Angew. Chem., Int. Ed.* **2015**, *54* (23), 6893−6895.
(72) Wang, Y.; Chen, C.; Lin, C. In Microchip based ion source powered by a lighter piezo-generator for mass-spectrometry detection. *10th IEEE International Conference on Nano/Micro Engineered and Molecular Systems* **2015**, 128−131.
(73) Barrie, L.; Platt, U. Arctic tropospheric chemistry: An overview. *Tellus, Ser. B* **1997**, *49*, 450−454.
(74) Barrie, L. A.; Bottenheim, J. W.; Schnell, R. C.; Crutzen, P. J.; Rasmussen, R. A. Ozone destruction and photochemical reactions at polar sunrise in the lower arctic atmosphere. *Nature* **1988**, *334*, 138−141.
(75) Finlayson-Pitts, B. J. Halogens in the Troposphere. *Anal. Chem.* **2010**, *82* (3), 770−776.
(76) Simpson, W. R.; von Glasow, R.; Riedel, K.; Anderson, P.; Ariya, P.; Bottenheim, J.; Burrows, J.; Carpenter, L. J.; Friess, U.; Goodsite, M. E.; Heard, D.; Hutterli, M.; Jacobi, H. W.; Kaleschke, L.; Neff, B.; Plane, J.; Platt, U.; Richter, A.; Roscoe, H.; Sander, R.; Shepson, P.; Sodeau, J.; Steffen, A.; Wagner, T.; Wolff, E. Halogens and their role in polar boundary-layer ozone depletion. *Atmos. Chem. Phys.* **2007**, *7* (16), 4375−4418.
(77) von Glasow, R.; Crutzen, P. J. Tropospheric halogen chemistry. In *Treatise on Geochemistry*; Holland, H. D., Turekian, K., Eds.; Elsevier Pergamon: San Diego, CA, 2007; Vol. *4.02*, pp 1−67.
(78) Simpson, W. R.; Brown, S. S.; Saiz-Lopez, A.; Thornton, J. A.; von Glasow, R. Tropospheric Halogen Chemistry: Sources, Cycling, and Impacts. *Chem. Rev.* **2015**, *115* (10), 4035−4062.
(79) Finlayson-Pitts, B. J.; Pitts, J. N., Jr. *Chemistry of the Upper and Lower Atmosphere—Theory, Experiments, and Applications*; Academic Press: San Diego, CA, 2000; p 969.
(80) McDow, S. R.; Mazurek, M. A.; Li, M.; Alter, L.; Graham, J.; Felton, H. D.; McKenna, T.; Pietarinen, C.; Leston, A.; Bailey, S.; Tong Argao, S. W. Speciation and atmospheric abundance of organic compounds in PM2.5 from the New York City area. I. Sampling network, sampler evaluation, molecular level blank evaluation. *Aerosol Sci. Technol.* **2008**, *42* (1), 50−63.
(81) Saffari, A.; Hasheminassab, S.; Shafer, M. M.; Schauer, J. J.; Chatila, T. A.; Sioutas, C. Nighttime aqueous-phase secondary organic aerosols in Los Angeles and its implication for fine particulate matter composition and oxidative potential. *Atmos. Environ.* **2016**, *133*, 112−122.
(82) Zheng, M.; Zhao, X. Y.; Cheng, Y.; Yan, C. Q.; Shi, W. Y.; Zhang, X. L.; Weber, R. J.; Schauer, J. J.; Wang, X. M.; Edgerton, E. S. Sources of primary and secondary organic aerosol and their diurnal variations. *J. Hazard. Mater.* **2014**, *264*, 536−544.
(83) Cavallo, G.; Metrangolo, P.; Milani, R.; Pilati, T.; Priimagi, A.; Resnati, G.; Terraneo, G. The halogen bond. *Chem. Rev.* **2016**, *116* (4), 2478−2601.
(84) Thirman, J.; Engelage, E.; Huber, S. M.; Head-Gordon, M. Characterizing the interplay of Pauli repulsion, electrostatics, dispersion and charge transfer in halogen bonding with energy decomposition analysis. *Phys. Chem. Chem. Phys.* **2018**, *20* (2), 905−915.
(85) Politzer, P.; Murray, J. S.; Lane, P. σ-Hole bonding and hydrogen bonding: Competitive interactions. *Int. J. Quantum Chem.* **2007**, *107* (15), 3046−3052.
(86) Desiraju, G. R.; Ho, P. S.; Kloo, L.; Legon, A. C.; Marquardt, R.; Metrangolo, P.; Politzer, P.; Resnati, G.; Rissanen, K. Definition of the halogen bond (IUPAC recommendations 2013). *Pure Appl. Chem.* **2013**, *85* (8), 1711−1713.
(87) Metrangolo, P.; Neukirch, H.; Pilati, T.; Resnati, G. Halogen bonding based recognition processes: A world parallel to hydrogen bonding. *Acc. Chem. Res.* **2005**, *38* (5), 386−395.
(88) Politzer, P.; Murray, J. S.; Clark, T. Halogen bonding and other sigma-hole interactions: A perspective. *Phys. Chem. Chem. Phys.* **2013**, *15* (27), 11178−11189.
(89) Clark, T.; Murray, J. S.; Politzer, P. The σ-hole coulombic interpretation of trihalide anion formation. *ChemPhysChem* **2018**, *19*, 3044−3049.
(90) Breugst, M.; Detmar, E.; von der Heiden, D. Origin of the catalytic effects of molecular iodine: A computational analysis. *ACS Catal.* **2016**, *6* (5), 3203−3212.
(91) Guha, S.; Sekar, G. Metal-free halogen (I) catalysts for the oxidation of aryl (heteroaryl) methanes to ketones or esters: Selectivity control by halogen bonding. *Chem.—Eur. J.* **2018**, *24* (53), 14171−14182.
(92) Gilday, L. C.; Robinson, S. W.; Barendt, T. A.; Langton, M. J.; Mullaney, B. R.; Beer, P. D. Halogen Bonding in Supramolecular Chemistry. *Chem. Rev.* **2015**, *115* (15), 7118−7195.
(93) Metrangolo, P.; Resnati, G. Halogen bonding: A paradigm in supramolecular chemistry. *Chem.—Eur. J.* **2001**, *7* (12), 2511−2519.
(94) Nagato, K.; Matsui, Y.; Miyata, T.; Yamauchi, T. An analysis of the evolution of negative ions produced by a corona ionizer in air. *Int. J. Mass Spectrom.* **2006**, *248* (3), 142−147.
(95) Sekimoto, K.; Sakai, M.; Takayama, M. Specific interaction between negative atmospheric ions and organic compounds in atmospheric pressure corona discharge ionization mass spectrometry. *J. Am. Soc. Mass Spectrom.* **2012**, *23*, 1109−19.
(96) Rondeau, D. DART Mass Spectrometry: Principle and Ionization Facilities. In *Direct Analysis in Real Time Mass Spectrometry*; Dong, Y., Ed.; Wiley-VCH Verlag GmbH & Co. KGaA: Weinheim, Germany, 2017; Chapter 2, pp 43−80, DOI: 10.1002/9783527803705.ch2.
(97) Skalny, J. D.; Mikoviny, T.; Matejcik, S.; Mason, N. J. An analysis of mass spectrometric study of negative ions extracted from negative corona discharge in air. *Int. J. Mass Spectrom.* **2004**, *233* (1), 317−324.
(98) Martínez-Lozano, P.; de la Mora, J. F. On-line Detection of Human Skin Vapors. *J. Am. Soc. Mass Spectrom.* **2009**, *20* (6), 1060−1063.
(99) Kaiho, T. *Iodine Chemistry and Applications*; John Wiley & Sons, Inc.: Hoboken, NJ, 2015; p 636.
(100) Palmer, D. A.; Ramette, R. W.; Mesmer, R. E. The hydrolysis of iodine: Equilibria at high temperatures. *J. Nucl. Mater.* **1985**, *130*, 280−286.
(101) Eigen, M.; Kustin, K. The kinetics of halogen hydrolysis. *J. Am. Chem. Soc.* **1962**, *84* (8), 1355−1361.

DOI: 10.1021/acsearthspacechem.9b00030
ACS Earth Space Chem. 2019, 3, 1315−1328

(102) Lin, C.-C. Volatility of iodine in dilute aqueous solutions. *J. Inorg. Nucl. Chem.* **1981**, *43* (12), 3229−3238.
(103) Sander, R. Compilation of Henry's law constants (version 4.0) for water as solvent. *Atmos. Chem. Phys.* **2015**, *15* (8), 4399−4981.
(104) Hayase, S.; Yabushita, A.; Kawasaki, M.; Enami, S.; Hoffmann, M. R.; Colussi, A. J. Heterogeneous reaction of gaseous ozone with aqueous iodide in the presence of aqueous organic species. *J. Phys. Chem. A* **2010**, *114* (19), 6016−6021.
(105) Pillar, E. A.; Guzman, M. I.; Rodriguez, J. M. Conversion of iodide to hypoiodous acid and iodine in aqueous microdroplets exposed to ozone. *Environ. Sci. Technol.* **2013**, *47* (19), 10971−10979.
(106) Teiwes, R.; Elm, J.; Handrup, K.; Jensen, E. P.; Bilde, M.; Pedersen, H. B. Atmospheric chemistry of iodine anions: Elementary reactions of I^-, IO^-, and IO_2^- with ozone studied in the gas-phase at 300 K using an ion trap. *Phys. Chem. Chem. Phys.* **2018**, *20* (45), 28606−28615.
(107) Zhou, W.; Zhao, J.; Ouyang, B.; Mehra, A.; Xu, W.; Wang, Y.; Bannan, T. J.; Worrall, S. D.; Priestley, M.; Bacak, A.; Chen, Q.; Xie, C.; Wang, Q.; Wang, J.; Du, W.; Zhang, Y.; Ge, X.; Ye, P.; Lee, J. D.; Fu, P.; Wang, Z.; Worsnop, D.; Jones, R.; Percival, C. J.; Coe, H.; Sun, Y. Production of N_2O_5 and $ClNO_2$ in summer in urban Beijing, China. *Atmos. Chem. Phys.* **2018**, *18* (16), 11581−11597.
(108) Le Breton, M.; Wang, Y.; Hallquist, Å. M.; Pathak, R. K.; Zheng, J.; Yang, Y.; Shang, D.; Glasius, M.; Bannan, T. J.; Liu, Q.; Chan, C. K.; Percival, C. J.; Zhu, W.; Lou, S.; Topping, D.; Wang, Y.; Yu, J.; Lu, K.; Guo, S.; Hu, M.; Hallquist, M. Online gas- and particle-phase measurements of organosulfates, organosulfonates and nitrooxy organosulfates in Beijing utilizing a FIGAERO ToF-CIMS. *Atmos. Chem. Phys.* **2018**, *18* (14), 10355−10371.
(109) Liao, J.; Sihler, H.; Huey, L. G.; Neuman, J. A.; Tanner, D. J.; Friess, U.; Platt, U.; Flocke, F. M.; Orlando, J. J.; Shepson, P. B.; Beine, H. J.; Weinheimer, A. J.; Sjostedt, S. J.; Nowak, J. B.; Knapp, D. J.; Staebler, R. M.; Zheng, W.; Sander, R.; Hall, S. R.; Ullmann, K. A comparison of Arctic BrO measurements by chemical ionization mass spectrometry and long path-differential optical absorption spectroscopy. *J. Geophys. Res.: Atmos.* **2011**, *116* (D14), D00R02.
(110) Bannan, T. J.; Bacak, A.; Muller, J. B. A.; Booth, A. M.; Jones, B.; Le Breton, M.; Leather, K. E.; Ghalaieny, M.; Xiao, P.; Shallcross, D. E.; Percival, C. J. Importance of direct anthropogenic emissions of formic acid measured by a chemical ionisation mass spectrometer (CIMS) during the winter clearflo campaign in London, January 2012. *Atmos. Environ.* **2014**, *83*, 301−310.
(111) Zhao, Y.; Chan, J. K.; Lopez-Hilfiker, F. D.; McKeown, M. A.; D'Ambro, E. L.; Slowik, J. G.; Riffell, J. A.; Thornton, J. A. An electrospray chemical ionization source for real-time measurement of atmospheric organic and inorganic vapors. *Atmos. Meas. Tech.* **2017**, *10* (10), 3609−3625.
(112) Kumar, M. R.; Prabhakar, S.; Kumar, M. K.; Reddy, T. J.; Vairamani, M. Negative ion electrospray ionization mass spectral study of dicarboxylic acids in the presence of halide ions. *Rapid Commun. Mass Spectrom.* **2004**, *18* (10), 1109−1115.
(113) An, X.; Zhuo, H.; Wang, Y.; Li, Q. Competition between hydrogen bonds and halogen bonds in complexes of formamidine and hypohalous acids. *J. Mol. Model.* **2013**, *19* (10), 4529−4535.
(114) Zabardasti, A.; Kakanejadifard, A.; Goudarziafshar, H.; Salehnassaj, M.; Zohrehband, Z.; Jaberansari, F.; Solimannejad, M. Theoretical study of hydrogen and halogen bond interactions of methylphosphines with hypohalous acids. *Comput. Theor. Chem.* **2013**, *1014*, 1−7.
(115) Zabardasti, A.; Tyula, Y. A.; Goudarziafshar, H. Interplay between N···H, N···X and Z···X interactions in the complex pairing of pyrazine with hypohalous acids: A NBO and QTAIM (quantum theory of atoms in molecules) analysis. *Bull. Chem. Soc. Ethiop.* **2017**, *31* (2), 241−252.
(116) Zabardasti, A.; Abbasi Tyula, Y.; Goudarziafshar, H. Theoretical investigation of molecular interactions between sulfur ylide and hypohalous acids (HOX, X = F, Cl, Br, and I). *J. Sulfur Chem.* **2017**, *38* (2), 119−133.
(117) Kinney, R. G.; Arndtsen, B. A. Decarboxylation with Carbon Monoxide: The Direct Conversion of Carboxylic Acids into Potent Acid Triflate Electrophiles. *Angew. Chem.* **2019**, *131* (15), 5139−5143.
(118) Candish, L.; Freitag, M.; Gensch, T.; Glorius, F. Mild, visible light-mediated decarboxylation of aryl carboxylic acids to access aryl radicals. *Chem. Sci.* **2017**, *8* (5), 3618−3622.
(119) Perry, G. J. P.; Quibell, J. M.; Panigrahi, A.; Larrosa, I. Transition-Metal-Free Decarboxylative Iodination: New Routes for Decarboxylative Oxidative Cross-Couplings. *J. Am. Chem. Soc.* **2017**, *139* (33), 11527−11536.
(120) Urbansky, E. T.; Cooper, B. T.; Margerum, D. W. Disproportionation kinetics of hypoiodous acid as catalyzed and suppressed by acetic acid-acetate buffer. *Inorg. Chem.* **1997**, *36* (7), 1338−1344.
(121) Huber, S. M.; Jimenez-Izal, E.; Ugalde, J. M.; Infante, I. Unexpected trends in halogen-bond based noncovalent adducts. *Chem. Commun.* **2012**, *48* (62), 7708−7710.
(122) Zierkiewicz, W.; Michalczyk, M. On the opposite trends of correlations between interaction energies and electrostatic potentials of chlorinated and methylated amine complexes stabilized by halogen bond. *Theor. Chem. Acc.* **2017**, *136* (10), 125.
(123) Liu, S.; Thompson, S. L.; Stark, H.; Ziemann, P. J.; Jimenez, J. L. Gas-phase carboxylic acids in a university classroom: Abundance, variability, and sources. *Environ. Sci. Technol.* **2017**, *51* (10), 5454−5463.
(124) Salthammer, T. Emissions of volatile organic compounds from products and materials in indoor environments. In *The Handbook of Environmental Chemistry*; Salthammer Pluschke, P., Ed.; Springer: Berlin, Germany, 2004; Vol. *4* (Part F), pp 37−71.
(125) Gallego, E.; Roca, F. J.; Perales, J. F.; Guardino, X. Assessment of Chemical Hazards in Sick Building Syndrome Situations: Determination of Concentrations and Origin of VOCs in Indoor Air Environments by Dynamic Sampling and TD-GC/MS Analysis. In *Sick Building Syndrome*; Abdul-Wahab, S. A., Ed.; Springer: Berlin, Germany, 2011; pp 289−333.
(126) Welke, J. E.; Zanus, M.; Lazzarotto, M.; Alcaraz Zini, C. Quantitative analysis of headspace volatile compounds using comprehensive two-dimensional gas chromatography and their contribution to the aroma of Chardonnay wine. *Food Res. Int.* **2014**, *59*, 85−99.
(127) Attaie, R.; Richter, R. L. Formation of volatile free fatty acids during ripening of cheddar-like hard goat cheese. *J. Dairy Sci.* **1996**, *79* (5), 717−724.
(128) Mahajan, S. S.; Goddik, L.; Qian, M. C. Aroma compounds in sweet whey powder. *J. Dairy Sci.* **2004**, *87* (12), 4057−63.
(129) Nance, M. R.; Setzer, W. N. Volatile components of aroma hops (*Humulus lupulus* L.) commonly used in beer brewing. *J. Brew. Distill.* **2011**, *2* (2), 16−22.
(130) Gan, H. H.; Yan, B.; Linforth, R. S. T.; Fisk, I. D. Development and validation of an APCI-MS/GC−MS approach for the classification and prediction of cheddar cheese maturity. *Food Chem.* **2016**, *190*, 442−447.
(131) Kaneda, H.; Kano, Y.; Kamimura, M.; Osawa, T.; Kawakishi, S. Analysis of long-chain fatty acids in beer by an HPLC-fluorescence detection method. *J. Agric. Food Chem.* **1990**, *38* (6), 1363−1367.
(132) Wang, W.; Feng, X.; Zhang, D.; Li, B.; Sun, B.; Tian, H.; Liu, Y. Analysis of volatile compounds in Chinese dry-cured hams by comprehensive two-dimensional gas chromatography with high-resolution time-of-flight mass spectrometry. *Meat Sci.* **2018**, *140*, 14−25.
(133) Guha, S.; Kazi, I.; Nandy, A.; Sekar, G. Role of Lewis Base Coordinated Halogen (I) Intermediates in Organic Synthesis: The Journey from Unstable Intermediates to Versatile Reagents. *Eur. J. Org. Chem.* **2017**, *2017* (37), 5497−5518.
(134) Juuti, S.; Norokorpi, Y.; Ruuskanen, J. Trichloroacetic acid (TCA) in pine needles caused by atmospheric emissions of kraft pulp mills. *Chemosphere* **1995**, *30* (3), 439−448.

DOI: 10.1021/acsearthspacechem.9b00030
ACS Earth Space Chem. 2019, 3, 1315−1328

(135) Heal, M. R.; Reeves, N. M.; Cape, J. N. Atmospheric concentrations and deposition of trichloroacetic acid in Scotland: Results from a 2-year sampling campaign. *Environ. Sci. Technol.* **2003**, *37* (12), 2627−33.
(136) Cardador, M. J.; Gallego, M. Haloacetic acids in swimming pools: Swimmer and worker exposure. *Environ. Sci. Technol.* **2011**, *45* (13), 5783−5790.
(137) Takino, M.; Daishima, S.; Yamaguchi, K. Determination of haloacetic acids in water by liquid chromatography-electrospray ionization-mass spectrometry using volatile ion-pairing reagents. *Analyst* **2000**, *125* (6), 1097−1102.
(138) Barnett, J. R.; Andrews, L. J.; Keefer, R. M. Trifluoroacetyl hypohalites as aromatic halogenating agents. *J. Am. Chem. Soc.* **1972**, *94* (17), 6129−6134.
(139) Henne, A. L.; Zimmer, W. F. Positive halogens from trifluoroacetyl hypohalites. *J. Am. Chem. Soc.* **1951**, *73* (3), 1362−1363.
(140) Carpenter, L. J. Iodine in the marine boundary layer. *Chem. Rev.* **2003**, *103* (12), 4953−4962.
(141) McFiggans, G.; Bale, C. S. E.; Ball, S. M.; Beames, J. M.; Bloss, W. J.; Carpenter, L. J.; Dorsey, J.; Dunk, R.; Flynn, M. J.; Furneaux, K. L.; Gallagher, M. W.; Heard, D. E.; Hollingsworth, A. M.; Hornsby, K.; Ingham, T.; Jones, C. E.; Jones, R. L.; Kramer, L. J.; Langridge, J. M.; Leblanc, C.; LeCrane, J. P.; Lee, J. D.; Leigh, R. J.; Longley, I.; Mahajan, A. S.; Monks, P. S.; Oetjen, H.; Orr-Ewing, A. J.; Plane, J. M. C.; Potin, P.; Shillings, A. J. L.; Thomas, F.; von Glasow, R.; Wada, R.; Whalley, L. K.; Whitehead, J. D. Iodine-mediated coastal particle formation: An overview of the Reactive Halogens in the Marine Boundary Layer (RHaMBLe) Roscoff coastal study. *Atmos. Chem. Phys.* **2010**, *10* (6), 2975−2999.
(142) Wang, P.; Zhao, N.; Tang, Y. Halogen Bonding in the Complexes of CH_3I and CCl_4 with Oxygen-Containing Halogen-Bond Acceptors. *J. Phys. Chem. A* **2017**, *121* (26), 5045−5055.
(143) Kaur, D.; Kaur, R.; Chopra, G. Comparison of hydrogen- and halogen-bonding interactions in the complexes of the substituted carbonyl compounds with hypohalous acids and monohaloamines. *Struct. Chem.* **2018**, *29* (1), 207−215.
(144) Wolf, M. E.; Zhang, B.; Turney, J. M.; Schaefer, H. F. A comparison between hydrogen and halogen bonding: The hypohalous acid−water dimers, $HOX.H_2O$ (X = F, Cl, Br). *Phys. Chem. Chem. Phys.* **2019**, *21* (11), 6160−6170.
(145) Cappelletti, D.; Candori, P.; Pirani, F.; Belpassi, L.; Tarantelli, F. Nature and stability of weak halogen bonds in the gas phase: Molecular beam scattering experiments and ab initio charge displacement calculations. *Cryst. Growth Des.* **2011**, *11* (10), 4279−4283.
(146) Yu, H.; Ren, L.; Huang, X.; Xie, M.; He, J.; Xiao, H. Iodine speciation and size distribution in ambient aerosols at a coastal new particle formation hotspot in China. *Atmos. Chem. Phys.* **2019**, *19* (6), 4025−4039.

DOI: 10.1021/acsearthspacechem.9b00030
ACS Earth Space Chem. 2019, 3, 1315−1328